Polyethylenimine-modified chitosan materials for the recovery of La(III) from leachates of bauxite residue

Zhao Feiping, Yang Ziqi, Wei Zongsu, Spinney Richard, Sillanpää Mika, Tang Juntao, Tam Michael, Xiao Ruiyang

DOI: 10.1016/j.cej.2020.124307

Polyethylenimine-modified chitosan materials for the recovery of La(III) from leachates of bauxite residue

Feiping Zhao [a,b,e], Ziqi Yang [a,b], Zongsu Wei [c], Richard Spinney [d], Mika Sillanpää [e], Juntao Tang [f,g], Michael Tam [g], Ruiyang Xiao [a,b,*]

[a] School of Metallurgy and Environment, Central South University, Changsha 410083, P.R. China

[b] Chinese National Engineering Research Centre for Control & Treatment of Heavy Metal Pollution, Changsha 410083, P.R. China

[c] Centre for Water Technology (WATEC), Department of Engineering, Aarhus University, Hangøvej 2, DK-8200 Aarhus N, Denmark

[d] Department of Chemistry and Biochemistry, the Ohio State University, Columbus, Ohio, 43210, U.S.A.

[e] Department of Green Chemistry, School of Engineering Science, LUT University, Mikkeli FI-50170, Finland

[f] College of Chemistry and Chemical Engineering, Central South University, Changsha, 410083, China

[g] Laboratory for Functional Colloids & Sustainable Nanomaterials, Department of Chemical Engineering, University of Waterloo, 200 University Avenue West, Waterloo, Ontario N2L 3G1, Canada

*To whom correspondence should be addressed. R. Xiao. Phone: +86–731–88830875; fax: +86–731–88710171; Email address: xiao.53@csu.edu.cn

ABSTRACT

The separation and recovery of rare earth elements (REEs) from leachates of bauxite residue has attracted increasing attention. Yet, the characteristics of bauxite residue leachates (low pH, low concentration of REEs, and co-existence of other trivalent ions) results in a longstanding challenge in the recovery of REEs. Here, we reported on the development of polyethylenimine (PEI) modified chitosan materials as efficient adsorbents for REE, La(III). The introduction of PEI brought abundant protonatable amino nitrogen atoms, which endows materials with excellent buffering capacity at extremely acidic pH. The PEI-chitosan materials can easily separate La(III) from Al(III), a major co-existing ion, with a separation factor of 3.1. The single-metal adsorption behavior showed fast and efficient adsorption capacity of 2.015 mmol/g for La(III). In binary systems, La(III) was preferentially adsorbed over Al(III) due to the higher degree of association with PEI. The FT-IR, XPS and EDS mapping results revealed that in the binding mechanism the N atoms form coordination bonds with La(III) by sharing an electron pair, resulting in eight-membered chelate rings. The PEI-chitosan materials also exhibited an excellent reusability with regeneration efficiency of 90% after 4 recycles. Overall, PEI-chitosan demonstrates that it is a viable and economical material for the separation and preconcentration of REEs from leachates of bauxite residue.

Key words

Rare earth elements, polyethylenimine, chitosan, preconcentration, bauxite residue, selective adsorption, La(III)

1. Introduction

The recovery of critical metals from stocks of landfilled industrial residues such as mine tailings, non-ferrous slag and bauxite residue (BR) is of beneficial both economically and for sustainability [1]. Particularly, the separation and recovery of rare earth elements (REEs) from secondary resources has attracted great attention in recent years due to the increasing REEs demand in many high-tech and futuristic applications [2]. Bauxite residue, also known as red mud, is a waste byproduct of the production of alumina from bauxite through the Bayer process [3]. Based on the current metallurgical technologies and bauxite composition, the alumina industry produces 45 million tons of bauxite residue per year worldwide [4]. The huge amount of bauxite residue stocks not only requires large areas of land as reservoirs, but also exhibits adverse effects to land ecosystem due to its high alkalinity [5,6]. However, bauxite residue contains critical and valuable REEs such as lanthanum (La(III)) after extraction [7]. Although at low concentrations, bauxite residue could still be considered as a highly potent source for valorization because of the huge existing stock and high production rate [3]. While Europe initiated Zero-Waste Valorization of Bauxite Residue (REDMUD) in Horizon 2020, which targets the vast new and stockpiled bauxite residues in the EU-28 countries [7], separation and recovery of the REEs from bauxite residue would be an important supplement to the supply of REEs.

There are many approaches to recover La(III) and other REEs from bauxite residue [8,9], but most need “dirty” acid leaching process to dissolve the REEs [10]. These leachate solutions possess three characteristics: low pH, low concentration of REEs, and other co-existing trivalent ions such as Al(III) and Fe(III), posing significant challenges in the recovery of La(III) [11]. Adsorption is considered as one of the most promising approaches to recover the very dilute La(III) from the leachate

with severe pHs, due to its low cost, ease of operation, pH tolerance, and possible selectivity [12]. Recently, various materials, such as carbon nanotube [13], silica [14], graphene [15], bentonite [16], clay [17], hydroxyapatite [18], $CuFe_2O_4$ [19], layered double hydroxide (LDH) [20], chitosan [21], cyclodextrin [22], and cellulose [23] have been employed as adsorbents for REEs recovery from diluted solutions. Chitosan, a linear polysaccharide obtained from the exoskeleton of crustacea, showed excellent performance in adsorption applications due to its high hydrophilicity (-OH groups) and good metal chelation ability (-NH_2 groups). More importantly, the abundant reactive amine and hydroxyl groups enable the easy modifications of chitosan structure by specific functional groups [24]. In our previous studies, we have modified chitosan by using Ethylenediaminetetraacetic acid (EDTA) [25], ethyleneglycol tetraacetic acid (EGTA) [26], and diethylenetriamine pentaacetic acid (DTPA) [24] as functional groups for enhanced heavy metal adsorption. Recently, Roosen et al. reported EGTA- and DTPA-modified chitosan-silica for selective scandium(III) adsorption [3]. However, these modifications occurred with the amine groups on chitosan, which are considered as the reactive adsorption sites for metal chelation [27]. Thus, the modifications would significantly reduce the intrinsic adsorption ability of chitosan. Therefore, to tackle the amine loss problem, a viable alternative would be to graft amino-rich macromolecules onto chitosan.

Polyethylenimine (PEI), a sterically branched polymer with larger numbers of amino groups, has high affinity towards REEs [28]. More importantly, one third of the atoms of PEI are protonatable amino nitrogen atoms, which endows the branched macromolecule with excellent buffering capacity at virtually any pH [29], even the severely acidic pH of bauxite leachates. These advantages show a great deal of potential for La(III) adsorption. Noted, PEI usually has to be immobilized on

substrates for water treatment application owing to its water solubility [30]. Recently, we have reported a PEI-modified cellulose nanocrystals (CNCs) for the highly efficient recovery of REEs from waters [23]. In that work, cellulose was first carboxylated through oxidation and further modified with PEI via carbodiimide-mediated amidation reaction. Despite the observed good performance, the synthesis of the CNCs was complicated and expensive (carbodiimide used [25]), due to the fact that functional groups (mainly hydroxyl) on pristine cellulose are relatively inert [31]. Together with the structural features of chitosan, we hypothesized that chitosan could be considered a better substrate for the immobilization of PEI [32]. Recently, several researchers have successfully utilized PEI-chitosan materials, which were prepared via self-assembling, for the controlled delivery of genes [33–35]. You *et al.* [36] synthesized a magnetic chitosan-PEI adsorbent for Congo red removal by using toxic epichlorohydrin [37] as cross-linker. More recently, Zeng *et al.* reported a PEI functionalized carboxymethyl chitosan composite adsorbent for selective removal of mercury [38]. In their study, relatively expensive carboxymethyl chitosan was selected as the substrate. To date, no studies extending the PEI-immobilized chitosan for the recovery of REEs have been reported.

Herein, we described a series of PEI-modified chitosan materials for the recovery of lanthanum from leachates of bauxite residue. The synthesis of PEI-chitosan using EDTA dianhydride as cross-linker was based on the design that EDTA dianhydride contains two anhydrides, one of which reacts with the amino of PEI while the other reacts with the amino of chitosan (Fig. **1**). In this study, the selectivity for the uptake of La (III) from nitrate leachates which contain equimolar La(III) and Al(III), the major cation in the leachates, was studied at various pHs and different initial concentrations. Further, the recovery kinetics and isotherms of the targeted REE by

PEI-chitosan materials in single-component system, the selective recovery of La(III) in binary systems, and the regeneration were all evaluated, aiming to shed light on the selective adsorption mechanisms.

2. Materials and methods

2.1. Materials

All regents were purchased from Sigma-Aldrich, and were used as received without further purification. Chitosan flakes, 80~90% deacetylated, showed a molecular weight (MW) ranging from 200,000 to 350,000 g/mol and a viscosity of 200-1800 MPa. The branched PEI had a MW of 70,000 g/mol in 50 wt% of water. Stock solutions of 1,000 mg/L were prepared by dissolving the appropriate amounts of $La(NO_3)_3 \cdot 6H_2O$ (>99.0% pure) and $Al(NO_3)_3 \cdot 9H_2O$ (analytical grade) in deionized (DI) water. Working solutions ranging from 5-500 mg/L were diluted from the stock solutions. The adjustment of pH from 2 to 7 was conducted by using 0.1 M NaOH and 0.1 M HNO_3, while working solutions at pH 0.5 and 1 were prepared by diluting the stock solutions with 1 M HNO_3. Prior to use, all breakers, flasks, and other glassware were immersed in 10% HNO_3 overnight for cleaning.

2.2. Synthesis of PEI-modified chitosan

The anhydride-mediated amidation reaction was used for grafting PEI onto chitosan [24]. A series of PEI-chitosan were synthesized by reacting 1.0 g chitosan with specified amounts of branched PEI at designated PEI:chitosan ratios (w/w), i.e., 0:1, 0.2:1, 0.5:1, 0.8:1, and 1:1. First, 1.0 g of chitosan and the specified amounts of PEI were dissolved in 20 mL of 10% (v/v) acetic acid and then diluted five times with methanol. Afterwards, 1.6 g of EDTA dianhydride synthesized according to Repo and

Sillanpää [24] was well suspended in methanol, then the suspension was added dropwise into the chitosan and PEI solution. The mixture was stirred at 300 rpm for 1 hr and then aged for 24 hr at room temperature. The resulted yellowish gel was filtered and mixed with ethanol under continuous stirring for another 5 hr. The residual EDTA was removed by washing the gel with excess NaOH solution (0.01 M). The product was successively rinsed with DI water and 0.1 M HCl to remove any unreacted PEI, followed by dialysis in DI water. Finally, the resulting swollen hydrogels were quick-frozen in liquid nitrogen and dried in a freeze-dryer (FreeZone, Labconco) under a high vacuum at -42 °C for 48 h. The detailed experimental conditions and yields are presented in Table **S1** in the supplementary information (SI).

2.3. Characterization

The elemental compositions of the materials were examined by a 2400 Series II CHNS/O Analyzer (PerkinElmer, USA). A Fourier transform infrared (FT-IR) spectrometer, Vertex 70 (Bruker, Germany) with a platinum ATR accessory, was employed to qualitatively determine the functional groups on the materials. Solid-state carbon-13 (^{13}C) magic angle spinning (MAS) NMR spectra were recorded with a ^{13}C frequency of 125.76 MHz on a Agilent-NMR-vnmrs 600 MHz spectrometer. A metrohm 809 Titrando autotitrator (Switzerland) was applied to quantitatively identify the amounts of the functional groups through a conductometric-potentiometric titration method. The morphologies of chitosan, PEI-modified chitosan materials before and after La(III) adsorption were observed by using a Jeol JSM-5800 scanning electron microscope (SEM) at an acceleration voltage of 20.0 kV. To investigate the La(III) distribution on the surface of PEI-chitosan materials, Elemental Mapping was simultaneously conducted during

SEM characterization by Thermo Scientific Ultra Dry SDD energy-dispersive X-ray spectroscopy (EDS) at an acceleration voltage of 5.0 kV. Thermogravimetric analyses (TGA) and derivative thermogravimetry (DTG) were performed using a NETZSCH TG-DTG STA449 F3 (Germany) at a heating rate of 10 °C per minute under a nitrogen atmosphere from 30 to 900 °C. X-ray photoelectron spectroscopy (XPS) was applied to identify the quantitative elemental, chemical state and functional group that exist within the PEI-chitosan materials by a Thermo ESCALAB 250XI (Thermo Fisher Scientific, UK).

2.4. La(III) and Al(III) uptake experiments

Batch La(III) and Al(III) adsorption experiments were conducted by mixing 10 mg of the adsorbent materials with 10 mL of La(III) or Al(III) solutions (dosage of 1 g/L) at designated initial concentrations ranging from 5 to 500 mg/L. The pH effect was investigated at an initial concentration of 1 mM in the pH range of 0.5-6.5. Strong alkaline solution was not studied to avoid the formation of La(III)/Al(III) hydroxides. The effect of contact time was studied at an initial La(III)/Al(III) concentration of 100 mg/L at pH 3.5. After each adsorption test, the adsorbent was separated from the aqueous solution using a 0.45 μm polypropylene syringe filter. The metal ion concentrations of the filtrates were analyzed at a wavelength of 333.749 nm (La) and 308.215 nm (Al) by an inductively coupled plasma emission spectrometer (ICP-OES) Model iCAP6300 Radial (Thermo Scientific, USA). All the uptake experiments were conducted in duplicate, and the uptake capacities (mmol/g) were calculated as:

$$q_e = \frac{(C_0 - C_e)}{M} V \quad (1)$$

where C_0 and C_e are the initial and equilibrium concentrations (mM) of the metal ions, respectively, while M (mg) and V (mL) represent the adsorbent weight (10 mg) and

the solution volume (10 mL), respectively.

2.5. Recovery of La(III) in binary La(III)-Al(III) systems

Al(III) is one of the dominant coexistent ions in the leachates of bauxite residue. The similarity of chemical properties between the trivalent metal ions raises the challenge to separate La(III) from the mixture of La(III) and Al(III) [10]. The competitive adsorption of La(III) and Al(III) onto PEI-chitosan was performed in binary systems, containing the equimolar La(III) and Al(III) ranging from 0.04 to 1.44 mM. An optimized pH of 3.5 was applied based on the results from single uptake results and an excessive contact time of 6 hr was used for the recovery of La(III) in binary systems.

2.6. Regeneration and preconcentration of La(III) in bauxite leachates

The regeneration and preconcentration of La(III) was also conducted in a native bauxite residue leachate, which was sampled at Xunwu county, Jiangxi province, China. The bauxite residue leachate sample was first membrane-filtered (0.45 μm) to remove the solid particles. The native bauxite residue leachate contained Na^{+} (826 mg/L), Ca^{2+} (652 mg/L), Al^{3+} (330 mg/L), Fe^{3+} (52 mg/L), and La^{3+} (4 mg/L), with an initial pH of 2.0. Aliquots of 500 mL native bauxite residue leachate were mixed with 1 g of adsorbents (dosage of 2 g/L) and agitated in a rotary oscillator at 200 rpm at room temperature for 6 hr. Subsequently, the solutions were separated by vacuum filtration, and the metal concentration in the filtrates were analyzed by ICP. The collected adsorbents were regenerated by using 10 mL of 1 M HNO_3 for 10 min, and then reused for La(III) uptake in succeeding cycles. All the uptake experiments were conducted in duplicate and the regeneration efficiency (RE%) of the adsorbent

materials were calculated as follows:

$$\mathrm{RE}\% = \frac{q_r}{q_0} \times 100\% \quad (2)$$

where q_0 and q_r are the La(III) uptake amounts (mmol/g) of the adsorbents before and after regeneration, respectively. The eluates (10 mL of 1 M HNO_3) which contained La(III) were directly reused for the next run regeneration to further enrich La(III). An enrichment factor was introduced to evaluate the La(III) preconcentration properties in the leachates of bauxite residue:

$$\text{Enrichment factor} = C_p/C_0 \quad (3)$$

where C_0 and C_p are the initial La(III) concentrations in feed solution (4 mg/L) and the final preconcentrated La(III) concentration in the eluate, respectively.

2.7. Breakthrough experiments

Two grams of PEI-chitosan(0.5:1) was packed into a column with inner diameter of 12 mm and the packed sample length was about 70 mm. An aqueous solution containing 330 mg/L of Al(III) and 4 mg/L of La(III) at pH 3.5 was then passed through the column with a flow rate of 1 mL/min at room temperature. The metal concentrations of the filtrates were measured by using an ICP-OES.

3. Results and discussion

3.1. Characterization

PEI-chitosan materials were prepared *via* an anhydride-mediated amidation reaction. The hypothesis was that the immobilization of PEI ligands on chitosan would result in hydrogel materials with high selectivity for La(III). The immobilization of the PEI ligands on chitosan proceeded by using EDTA dianhydride as a cross-linker, where one anhydride group of EDTA dianhydride reacts with the

available amino groups on chitosan moieties while the other reacts with the primary amino groups of PEI. To investigate PEI-chitosan ratio effects on the La(III) uptake performance, five PEI-chitosan materials labelled as PEI-chitosan(0:1), PEI-chitosan(0.2:1), PEI-chitosan(0.5:1), PEI-chitosan(0.8:1), and PEI-chitosan(1:1), were fabricated by varying their mass ratios.

A summary of the synthesis and elemental analysis is given in Table **S1**. The mass yield increased with the amount of PEI, and reached a maximum at PEI-chitosan(0.5:1) (79.35%, Table **S1**). The product weight decreased when PEI-chitosan ratio was above 0.5:1 g due to the fact that the excessive PEI might generate the byproduct PEI-EDTA which is water soluble, leading to a lower mass yield. As shown in Fig. **S1**, the color of the generated PEI-chitosan hydrogels increased with the PEI amount from light to dark yellowish. As presented in Table **S1**, the significant difference in the nitrogen content between PEI-chitosan(0:1) and PEI-chitosan materials verified the successful introduction of PEI into the materials, since nitrogen is abundant in PEI (*ca.* one third of atoms in PEI are nitrogen) [39]. It was clearly observed that the nitrogen content dramatically increased from PEI-chitosan(0:1) to PEI-chitosan(0.5:1), but the increase from PEI-chitosan(0.5:1) to PEI-chitosan(1:1) was not significant, even though the PEI dosage of the latter was twice that of PEI-chitosan(0:1). As shown in Table **S2** and **S3**, a cost analysis based on the raw material cost and yield was further carried out. The cost analysis results suggest that the pilot-scale cost of PEI-chitosan(0.5:1) is the lowest (6.63 $/kg) among the four PEI-chitosan materials. Therefore, from an atom economy perspective, PEI-chitosan(0.5:1) could be considered as the most cost-effective among the PEI-chitosan products.

The morphologies of the series of PEI-chitosan hydrogels were characterized by

SEM (Fig. **2**). All these hydrogels showed porous structure with typical network of two-dimensional sheet-like pore walls, which were similar to other cross-linked polysaccharide hydrogels after freeze-drying as previously reported [23,28,40]. Notably, the porous structure started to collapse at the dosage of 0.8 g PEI (Fig. **2d**), and became totally loose structure in PEI-chitosan(1:1) (Fig. **2e**). Further, the PEI-chitosan hydrogel after freeze-drying was light enough to stand on the stamens of a flower due to the porous structure (Fig. **S2a**). The highest yield hydrogel, PEI-chitosan (0.5:1), showed a dense and orderly network structure with smooth pore wall (Fig. **S2b-d**).

FT-IR spectra were used to confirm the anhydride-mediated amidation reaction and the presence of the additional functional groups on the modified chitosan (Fig. **3**). In comparison with the pristine chitosan, PEI-chitosan(0:1), namely EDTA-modified chitosan, showed characteristic features at 1634 and 1731 cm^{-1}, which are assigned to the carbonyl groups of the amides and carboxylic groups, respectively [24]. Notably, three intense peaks at 1640, 1564, and 1446 cm^{-1} in the spectra of PEI-chitosan(0.2:1, 0.5:1, 0.8:1 and 1:1) (Fig. **3** and S**3**) verified the presence of the amide bond and amino groups [41,42]. In addition, PEI-chitosan materials exhibited wider bands than pristine chitosan in the range of 3050-3650 cm^{-1}, due to the coexistence of O-H and N-H groups in the PEI-chitosan materials [43]. The ^{13}C solid-state-MAS NMR spectra of chitosan and PEI-chitosan(0.5:1) are presented in Fig. **4**. The top spectrum (Fig. **4a**) is the one for pristine chitosan. The signals at 55.6, 59.1, 83.2, and 103.1 ppm were assigned to C2, C6, C4, and C1 of the pyranose ring, respectively. A strong peak at 74.9 ppm could be assigned to overlapping C3 and C5 [44]. After immobilization of PEI onto the chitosan backbone, new resonances were observed (Fig. **4b**). The strong signal at 164.2 ppm can be attributed to the amidic carbons (C9). Further, a new

signal at 36.8 ppm is ascribed to the CH_2 carbons (C10/11) of the grafted PEI. The observed C9, C10, and C11 signals were consistent with the reported PEI-modified cellulose [28], indicating the successful amidation reaction and the presence of PEI in the synthetic product. All these facts confirmed the successful introduction of PEI groups in the materials through an anhydride-mediated amidation reaction.

The surface chemical property changes of chitosan during EDTA- and PEI-modification were analyzed by XPS (Fig. **5**). The carbon core line measured for chitosan (panel C 1s, Fig. **5**) showed three splitting peaks of binding energy (BE) at 287.86, 286.3, and 284.84 eV, which could be assigned to the carbonyl (C=O), carbon bound to oxygen (C-O) and nitrogen (C-N), respectively [45]. The presence of carbonyl in chitosan could be attributed to the residual N-acetyl groups after 80-90% deacetylation of chitin. After EDTA-modification (PEI-chitosan(0:1)), it is clearly observed that both C=O and C-O peaks were enhanced, suggesting the successful introduction of -COOH groups in the PEI-chitosan(0:1). In the C 1s spectrum of PEI-chitosan(0.5:1), the BE peak at 284.81 eV for C-N was found to be significantly increased, in comparison with PEI-chitosan(0:1). This was in a good agreement with the other PEI-modified materials [46]. Moreover, the successful immobilization of PEI could also be clearly seen from the nitrogen core lines (panel N 1s, Fig. **5**). The splitting of BE peaks at 399.83 and 399.02 could correspond to the typical imine and tertiary amine groups in PEI, in good agreement with literature [46,47]. Importantly, the much sharper BE peaks at 401.51 eV for PEI-chitosan(0.5:1) compared to both pristine chitosan and PEI-chitosan(0:1), could be assigned to the protonation of the abundant aliphatic amines in PEI [46].

In order to determine amounts of weak acid and weak base in polysaccharide materials, the quantitative analyses of the amounts of specific carboxylic and amine

groups in each material were conducted by conductometric–potentiometric titration. The titration curves are shown in Fig. **6** and Fig. **S4**. Different numbers of titration end points were found in various materials. For example, PEI-chitosan(0.5:1) showed four end points, which divided the conductivity curve into five regions: strong acid neutralization, weak acid neutralization, primary amine dissociation, secondary amine dissociation, and excessive strong base (Fig. **6d**, from left to right). Based on the amounts of NaOH titrated in each stage, the specific amounts of the functional group could be estimated and the results were summarized in Table **1**. In PEI-chitosan(0:1), the high amount of -COOH (5.38 mmol/g) could be due to the modification by only EDTA ligand. When PEI were introduced, the -COOH amounts were dramatically reduced to 1.4-1.9 mmol/g, since a larger number of carboxylic groups were involved in the amidation reaction with amino groups. The total amino groups increased greatly from PEI-chitosan(0.2:1) to PEI-chitosan(0.5:1), but the increase from PEI-chitosan(0.5:1) to PEI-chitosan(1:1) were not significant. The titration result was in a good agreement with the results of elemental analyses. Interestingly, there are many more primary amino than secondary amino groups in the pristine PEI, but the difference between the two were not pronounced in PEI-modified chitosan materials. A similar phenomenon was observed in the reported PEI-CNCs due to the fact that primary amino groups react with carboxylic groups in the amidation reaction [23,28]. The PEI-modified chitosan materials also displayed obviously different thermal behaviors compared to pristine chitosan and EDTA-modified chitosan. As shown in Fig. **S5**, the pristine chitosan exhibited a characteristic decomposition with an onset temperature of 242 °C and an end temperature of 379 °C (a sharp DTG peak at 292 °C), consistent with previous reported chitosan [25]. For PEI-chitosan(0:1), the weight loss started at a lower temperature, 165 °C, and ended at 362 °C with a DTG

peak of 201 °C, suggesting that the modification by only EDTA ligands significantly reduced the thermal stability of chitosan. Similar reduced stability phenomenon was also observed in the other carboxylic group modified polysaccharide materials (TEMPO-CNCs) [23]. Besides the typical chitosan pyrolysis (242-379°C), PEI-modified chitosan displayed a new degradation at higher temperatures of 306-452 °C, due to the decomposition of the PEI macromolecule chains, same as the reported PEI membrane [43]. This indicated that the PEI-functionalization might enhance the thermal stability of chitosan.

3.2. Effect of pH and selectivity

Prior to the adsorption tests, blank control experiments (*i.e.,* experiments without absorbent materials) were conducted to investigate the losses of metal ions during the sample filtration procedure. As shown in Fig. **S6**, after filtration, the losses of both of Al(III) and La(III) were less than 2% in the pH ranging from 1 to 3.6. Thus, the effect of the filtration procedure is negligible during the adsorption procedure. This could be attributed to the low affinity between the pristine polypropylene and metal ions. A similar phenomenon has been reported by Mostafa *et al.* [48].

The recovery of La(III) was investigated as a function of pH, since pH is a significant factor for adsorption. The pH affects not only the protonation of the functional groups immobilized on the surface of the sorbents but also the speciation of metal ions in aqueous media [37]. It is well known that the precipitation of $Al(OH)_3$ and $La(OH)_3$ would occur when pH increased. In order to eliminate the interference of precipitation on the calculation of adsorption amount, the pH at which precipitation occurs was calculated based on their respective solubility product constants ($Ksp[Al(OH)_3] = 2.0 \times 10^{-31}$ and $Ksp[La(OH)_3] = 2.0 \times 10^{-21}$) [49–51]. As shown in

Text **S1**, based on the K_{sp} calculations, the precipitation pH values were estimated to be 3.88 for $Al(OH)_3$ and 7.26 for $La(OH)_3$, respectively. At pH above these values, precipitation has to be taken into account in the removal efficiency. The influence of the equilibrium pH was firstly investigated in single-metal solutions of Al(III) and La(III), and the results were shown in Fig. **S7**. For most of the studied adsorbents, the Al(III) removal efficiency increased from pH 0.9 to 3 reaching an asymptotic value. Notably, a quite significant increase of Al(III) removal efficiency was observed at pH beyond 3.5 for all the five investigated materials (Fig. **S7a-e**). This could be attributed to the fact $Al(OH)_3$ precipitation occurs at pH 3.88. A similar increase trend and asymptotic plateau were observed in La(III) removal, but the precipitation increase was not found due to the fact that the $La(OH)_3$ precipitation pH (7.26) was larger than the tested pHs. Further, the asymptotic values of La(III) were much higher than those of Al(III), indicating the potential for separation of La(III) from Al(III).

To verify the selectivity towards lanthanum, the adsorption of metal ions were carried out in a binary and equimolar solution of Al(III) and La(III) ($C_{initial}$ = 1 mM for each metals). In Fig. **7**, metal removal is presented as a function of the equilibrium pH for both PEI-chitosan(0:1) (Fig. **7a**) and PEI-chitosan(0.5:1) (Fig. **7b**). It is clear that the affinity of PEI-chitosan(0:1) towards Al(III) and La(III) are quite close, leading to difficulty in the separation of these ions. This could be attributed to their close stability constants with EDTA (EDTA-Al(III) 16.13, EDTA-La(III) 15.50) [52], which is the major functional group in PEI-chitosan(0:1). In the case of PEI-chitosan(0.5:1), about 70% of La(III) removal was obtained at pH 1.9, a pH at which almost no Al(III) was adsorbed. The maximal adsorption for La(III) was reached at pH 3.5, a pH at which almost four times more La(III) was adsorbed compared Al(III). This significant difference in the adsorption efficiencies for La(III)

and Al(III) reveals that PEI-chitosan(0.5:1) can be used for separation. The selectivity behavior of PEI-chitosan(0.5:1) should be attributed to the introduction of PEI in the materials, which contains large numbers of amino groups with high affinity towards REEs [53,54]. The pH for maximal La(III) adsorption, pH of 3.5, was selected for the further adsorption experiments.

It should be admitted that one could consider adjusting pH as an alternative to separate Al(III) and La(III), since Al(III) precipitation starts at lower pH in comparison with La(III). However, the hydrolysis of Al(III) results in $Al(OH)_3$, which is an efficient inorganic coagulant and is able to capture La(III) via coagulation. This would make the separation of Al(III) and La(III) even more difficult. Further, in the practical leachates of bauxite residue, the relative amount of Al(III) is significantly larger than that of La(III). It is therefore expected that the coagulation of La(III) will be more pronounced in environmental samples, indicating that precipitation would not be considered as an appropriate method to isolate La(III) from Al(III). Thus, the selectivity feature of our PEI-chitosan materials will be more desirable.

3.3.Adsorption kinetics

The kinetics of La(III) adsorption were investigated with the PEI-chitosan materials in single-metal nitrate solutions of La(III) and Al(III), with contact time ranging from 5 to 600 min. As shown in Fig. **8a**, equilibrium was reached within 120 min, which was observed as the beginning of a plateau in the adsorption curve. The adsorption in the initial stage was fast due to the abundant vacant adsorption sites [24]. The plateau values for PEI-chitosan materials were found as following order: PEI-chitosan(0.5:1) > PEI-chitosan(1:1) > PEI-chitosan(0.8:1) > PEI-chitosan(0.2:1) > PEI-chitosan(0:1). This order are in good agreement with the amount of amino groups

(-NH_2) (Table **1**, 4.53 mmol/g for PEI-chitosan(0.5:1), 4.44 mmol/g for PEI-chitosan(1:1), 4.24 mmol/g for PEI-chitosan(0.8:1), 2.01 mmol/g for PEI-chitosan(0.2:1), and 0 mmol/g for PEI-chitosan(0.5:1), respectively), indicating that the amino groups play dominant roles in the uptake of La(III) during the adsorption. Similar phenomenon was also observed in previously reported PEI-modified cellulose nanocrystals [23]. The time effect on Al(III) was also compared with that of La(III). As shown in Fig. **S8**, the adsorption of Al(III) was also fast and plateaued after 120 min. However, only 20%-40% of Al(III) was adsorbed, which is significantly lower than that of La(III) (60%-90%). This might be due to the higher affinity of amino groups towards La(III) in comparison with Al(III) [55]. To fully ensure adsorption equilibrium, a contact time of 360 min was chosen for all the following experiments [52,56].

In order to elucidate the adsorption rate constants, the kinetic data were further fit by using the pseudo first-order and pseudo second-order models. The pseudo first-order model, which is widely used for the adsorption in liquid/solid systems, is expressed as [26,57]:

$$\log(q_e - q_t) = \log(q_e) - \frac{k_1}{2.302} t \quad (4)$$

The pseudo second-order model, which assumes that the chemical surface reaction is the rate-limiting step, is expressed as [58]:

$$\frac{t}{q_t} = \frac{1}{k_2 q_e^2} + \frac{1}{q_e} t \quad (5)$$

where q_t and q_e (mmol/g) are the uptake amounts of La(III) at time t (min) and at equilibrium, respectively, while k_1 (/min) and k_2 (g/mmol min) are the adsorption rate constants of the pseudo first-order and pseudo second-order models, respectively. As shown in Fig. **S9** and Table **S4**, the pseudo first-order model did not fit the adsorption of La(III) well. The calculated q_e values could not match with the experimental values,

and all the correlation coefficients (R^2) were less than 0.9. However, according to Fig. **8b** and Table **S5**, it is evident that the pseudo second-order model gave the perfect fit to the experimental data of La(III) onto PEI-chitosan materials. The goodness of fit was reflected by the fitting curves and the high correlation coefficient of R^2 values. These all indicate that chemical surface adsorption is the rate-limiting step [23,59,60] in La(III) adsorption recovery for all studied materials. Importantly, the rate constant of PEI-chitosan(0.5:1) towards La(III) (0.372 g/mmol min) was almost three times higher than that of PEI-chitosan(0:1) (0.134 g/mmol min), suggesting that the introduction of PEI not only enhanced the La(III) adsorption efficiency, but also accelerated the adsorption kinetics.

3.4. Adsorption isotherms

To elucidate the adsorption characteristics of metals onto PEI-chitosan materials, such as uptake capacity and interactions between the metals and adsorption sites, two classic isotherm models (Langmuir and Freundlich) were applied to fit the experimental data. The Langmuir model, which assumes that monolayer adsorption occurs on a homogeneous surface, is given as [26]:

$$q_e = \frac{q_m K_L C_e}{1+K_L C_e} \quad (6)$$

The Freundlich isotherm predicts a heterogeneous adsorption and an energetically heterogeneous surface without a saturation of adsorption sites [37]:

$$q_e = K_F {C_e}^{1/n_F} \quad (7)$$

where q_e (mmol/g) and C_e (mM) are the metal uptake amount and equilibrium metal concentration, respectively, while q_m (mmol/g), K_L (L/mmol), and K_F (mmol^{1-n} L^n/g) represent the maximum metal adsorption capacity, the Langmuir energy constant, and the heterogeneity factor obtained after nonlinear fitting, respectively.

The isotherm fitting by the two models and the isotherm constants determined are presented in Fig. **9** and Table **S6**, respectively. Obviously, the experiment data fit better to the Langmuir model with correlation coefficient R^2 values of 0.995-0.996, higher than the Freundlich model (0.949-0.973), suggesting that the adsorption of Al(III) and La(III) onto PEI-chitosan(0.5:1) was better described by the Langmuir model. The Langmuir model possesses a finite saturation limit, which could calculate the maximum adsorption capacity $q_{m,cal}$. As shown in Table **S6**, the Langmuir model calculated $q_{m,cal}$ and the experimental $q_{m,exp}$ were quite similar to each other (±0.03 mmol/g), suggesting that Langmuir model could predict the maximum adsorption capacity in the single metal systems [61]. Moreover, the higher surface affinity K_L value of La(III) (2.62 L/mmol) than Al(III) (2.016 L/mmol) reveals that PEI-chitosan(0.5:1) has better affinity towards La(III) in comparison with Al(III). The affinity difference could also be found from the difference of q_m values between La(III) (2.015 mmol/g) and Al(III) (1.577 mmol/g). However, this q_m difference in single-metal adsorption system was not significant. Therefore, in order to investigate the selectivity ability of PEI-chitosan materials, it is necessary to carry out the simultaneous adsorption tests in Al(III)-La(III) binary systems.

The maximum adsorption capacities of La(III) onto PEI-chitosan(0.5:1) and other commonly used adsorbents are summarized in Table **2**. The high q_m values of PEI-chitosan(0.5:1) are very comparable to most of the reported adsorbents except for the Mg–Fe-LDH-Cyanex-272. The extraordinarily high La(III) uptake ability of Mg–Fe-LDH-Cyanex-272 could be attributed to the abundant inner layer anion exchange sites in the adsorbent. However, this LDH material also possessed the drawback of relatively low regeneration ability [20]. It should be noted that the q_m value of PEI-chitosan(0.5:1) was much higher than our previously reported for PEI-cellulose

nanocrystal [23]. This might be attributed to the fact that there are more active reaction sites on chitosan in comparison with cellulose, resulting in more PEI loading on the substrate. All of these suggested that the PEI-modified chitosan materials are efficient and promising adsorbents for REEs recovery.

3.5. Simultaneous adsorption studies of Al(III)-La(III) binary system

To investigate the selective adsorption of REEs onto PEI-chitosan materials, Al(III)-La(III) binary adsorption experiments were performed in aqueous solutions containing equimolar initial concentrations of Al(III) and La(III) ranging from 0.04 to 1.4 mM at pH 3.5, which was below the pH onset points of the precipitation of the two ions. As shown in Fig. **10**, in the binary metal systems, the adsorption capacities of both Al(III) and La(III) were found to be lower than their corresponding values in single metal systems (Fig. **9** and Table **S6**). This revealed the competition between Al(III) and La(III) when they co-exist. Interestingly, it is noted that Al(III) adsorption was more inhibited by the presence of La(III). Specifically, at the initial concentration of 1.4 mM in binary system, the adsorption capacity of Al(III) (0.359 mmol/g) was much lower than that of La(III) (1.105 mmol/g), indicting a separation factor of 3.1. This could be due to the bindings groups on the surface having a different stability constant with each metal ions [55,62]. The difference between the uptake of Al(III) and La(III) was not significant in single metal systems (Fig. **9**), however, in the case of binary systems, La(III) was preferentially adsorbed over Al(III) when the metal ions were present in equimolar concentration (Fig. **10**). On the whole, it can be concluded that the PEI-chitosan material possessed higher affinity toward La(III) than Al(III) and could be applied to separate La(III) from other trivalent metal ions such as Al(III).

3.6. Adsorption mechanisms

The elemental distribution for PEI-chitosan(0.5:1) after simultaneous adsorption of La(III) and Al(III) is illustrated in Fig. **11**. The bright colorful elemental signal spots show that La(III) was well distributed over the surface of PEI-chitosan(0.5:1), indicating the successful adsorption of La(III) and the uniform and well-distributed active sites on the sorbent. Importantly, it is noticed that the distribution of La(III) agreed with the signal spots of nitrogen and oxygen, especially in the area of a low nitrogen and oxygen signals where there is lower lanthanum loading. It is noted that significantly fewer aluminum signal spots were observed compare with lanthanum in the EDS mapping (Fig. **11**), even though equimolar La(III) and Al(III) co-existed in the initial solution. This result was further confirmed by EDS analysis spectra, where much larger area of La peak was observed compared to the Al peak (Figure **S10**). The high content of La and low content of Al are in a good agreement with the results of adsorption capacities of La(III) and Al(III) obtained in binary systems (Figure **10**).

To further clarify the interaction between the adsorption sites and La(III), the FT-IR of PEI-chitosan(0.5:1) before and after La(III) was compared in Fig. **12 A**. The peaks at 1640 and 1564 cm^{-1} in the spectrum of PEI-chitosan(0.5:1), assigned to the bending vibrations of N-H from amide bond and amino groups, were found to be significantly reduced in the PEI-chitosan(0.5:1)-La(III) spectrum, suggesting that N-H groups were involved in the La(III) adsorption [42]. Moreover, the peak at 1256 cm^{-1} assigned to C-O from carboxyl groups had obviously declined after La(III) loading, revealing that C-O participated in the adsorption as well [63]. It is noted that the band at 3050-3600 cm^{-1} assigned the overlapping stretching vibration of amine ($-NH_2$) and carboxyhydroxyl (-OH) groups in the pristine PEI-chitosan(0.5:1) became

significantly weaker after La(III) loading, revealing the interaction between La(III) and amine/carboxyhydroxyl groups [64].

As shown in **Fig. 1**, there are multiple functional groups present in PEI-chitosan(0.5:1), including three types of amine groups (primary, secondary, and tertiary amine groups) from PEI molecules and carboxylate groups from EDTA moieties. To determine which functional groups contribute to La(III) adsorption, the surface chemical properties of PEI-chitosan(0.5:1) before and after La(III) adsorption were compared *via* XPS (Fig. **12**). After La(III) adsorption, the intensity of the BE peak of C1s at 286.3 eV (Fig. **12c**) assigned to C-O was significantly reduced (Fig. **12e**), while the other two peaks of C=O and C-N showed minimal changes. Further, the BE peak of N1s at 401.51 eV corresponding to protonated primary amine groups (Fig. **12d**) became much weaker after La(III) adsorption, while the signal of secondary amino groups did not show significant reduction (Fig. **12f**), indicating the primary amino groups (-NH_2) give the main contribution for La(III) recovery. Both of these confirmed that C-O and -NH_2 groups were involved in La(III) binding, in a good agreement with the conclusion obtained from FT-IR results. Similar reduction of BE peaks was also observed for the previously reported alginate@PEI beads after Cr(VI) adsorption [65]. In La3d spectrum of the La(III) loaded adsorbent (Fig. **12**B), the BE peaks at 851.65 eV and 834.86 eV were assigned to La 3d3/2 and La 3d5/2 respectively, providing strong evidence of La(III) being successfully adsorbed on PEI-chitosan(0.5:1). Further, the satellite peaks of La3d (856.54 eV for La 3d3/2 and 837.43 eV for La 3d5/2) can be explained in terms of the transfer of a lone pair of electrons from N or O to La(III) suggesting the presence of the La-N/La-O coordination bond [66]. All these are consistent with our hypothesis that the primary amino groups from PEI molecules and carboxylate groups from EDTA moieties are

the dominant sites for La(III) adsorption. Since all cases in this study were performed in acid media, the coordination for La(III) ions is proposed as follows:

$$\mathrm{RNH_3^+ + La^{3+} \rightleftharpoons La(RNH_2)^{3+} + H^+} \quad (8)$$

$$\mathrm{RH_iEDTA^{i-3} + La^{3+} \rightleftharpoons La(REDTA) + iH^+} \quad (9)$$

On the basis of our results above, a possible adsorption mechanism of La(III) onto bifunctional primary amino and carboxylate groups of PEI-chitosan materials was proposed and described in Fig. **13**. It appears that each component of PEI-chitosan has a crucial role in its functioning: the chitosan chains act as the backbone of the materials; the EDTA-moieties play roles as not only cross-linkers, but also as active sites for REE chelating; on the other hand, the immobilized branched PEI molecules with abundant amino groups significantly enhanced the REE adsorption ability. Importantly, the protonatable amino nitrogen atoms, which endows the materials with excellent buffering capacity at virtually any pH [29], including the severe pH of bauxite leachates. Hong et al. reported that La(III) ions formed a five-membered chelated ring with polydopamine via the oxygen atoms on two phenolic hydroxyl groups [67]. In the structure of PEI, the N atom form a coordination bond with La(III) by sharing an electrons pair, and two amino groups are possible to form eight-membered chelate rings with La(III) ions after La(III) chelating (Fig. **13**). In addition, the binding affinities were determined at the SMD/M06-2X/SDDAll level of theory (Fig. **S11**). The binding affinities were determined using EDTA and a methyldiethylaminoamine (triamine) as models for the two possible chitosan binding sites. La^{3+} show a preference for the triamine site, $\Delta G°$ of -15.0 kcal/mol, while Al^{3+} also shows a preference for the triamine but by only -5.1 kcal/mol. The large difference in energy should lead to a preferential binding of La^{3+} leading to its selective chelation and removal from solutions.

3.7. Regeneration and preconcentration of La(III)

From the practical point, reusability is an important feature of a promising adsorbent material. More importantly, with the purpose of recovery of REEs from very diluted solutions, efficient REE enrichment ability is also necessary. In this study, La(III) was firstly desorbed from the spent PEI-chitosan material using 1 M HNO_3. As shown in Fig. **14**, the regenerated PEI-chitosan was reused for the next run adsorption of La(III), meanwhile the eluate (1 M HNO_3) which contained 50-fold preconcentrated La(III) was directly used for the next run regeneration. In most of regeneration studies, the eluent was only used once and the enrich factors were not high [22–24,68]. This is the first time to use the concept to recycle the eluate. The eluent used in this study is 1 M HNO_3 with high solubility of $La(HNO_3)_3$ (> 10 g/L) [69]. Thus, it is theoretically feasible to recycle eluate and the desorbed La(III) can be accumulated in the eluate. Table **3** shows that the regeneration efficiency for La(III) remained above 90% for the first four cycles, suggesting that 1 M HNO_3 is an efficient eluent in this case and PEI-chitosan materials are stable in nitric acid. Significantly, the enrichment factor of the first run was found to be 47.99, which was very close to the ideal value of 50, indicating that the material is suitable for the preconcentration of La(III) in low concentration of REEs. After 10 runs, the La(III) in the eluate was accumulated to be 1.2 g/L, which could be easily utilized for the succeeding REE metallurgical processes.

3.8. Column adsorption and breakthrough curves

The breakthrough curves for the adsorption of binary component solutions of Al(III) (330 mg/L) and La(III) (4 mg/L) at pH 3.5 and a flow rate of 1 mL/min are

shown in Fig. **15**. As shown in Fig. **15**, different adsorption behaviors for Al(III) and La(III) in the fix-bed column were observed. The breakthrough curve of Al(III) reached the penetration point at 5 min and reached depletion point within 30 min, while La(III) reached penetration point at 600 min and reached depletion point within 900 min. The comparison revealed that the adsorption capacity of Al(III) was much lower than La(III) in dynamic binary adsorption. Moreover, the large difference between the two penetration point values of Al(III) and La(III) guarantees the efficient separation of the individual species. This indicates that PEI-chitosan(0.5:1) is a promising material for the separation of La(III) from Al(III) at the concentrations of practical leachates of bauxite residue.

Conclusions

In this study, a series of PEI-modified chitosan materials were fabricated by a facile approach using EDTA dianhydride as the cross-linker. PEI modification introduced abundant amino groups which have been verified as one of the most efficient functional groups for REE coordination. It was found that in the pH range of 1-3.5 the PEI-chitosan material could successfully separate La(III) from Al(III). PEI-chitosan(0.5:1) was the optimal material taking into account of both the efficiency and atom economy. Further, the introduction of PEI not only enhanced the La(III) adsorption efficiency, but also accelerated the adsorption kinetics. In single-metal adsorption system, PEI-chitosan(0.5:1) exhibited high absorptivity toward La(III) (q_m 2.015 mmol/g). Interestingly, the difference between the uptake of Al(III) and La(III) was not significant in single metal systems, but in the case of Al(III)-La(III) binary system, La(III) was preferentially adsorbed over Al(III) when the metal ions were present in equimolar concentration. More importantly, the

regeneration of the spent PEI-chitosan(0.5:1) and the preconcentration of La(III) were realized via simultaneous recycling the adsorbent and eluent. Our results suggested that this efficient material can be extended to the applications for the recovery of REEs from other stocks of mine residues such as tungsten and apatite residues.

Acknowledgements

Funding from National Nature Science Foundation of China (No. 21976212) and National Science Fund for Distinguished Young Scholars (No. 51825403) is gratefully acknowledged. Authors also wish to thank Dr. Shengxi Wu (CSU) for constructive discussion. We also thank the referees for their constructive comments and suggestions.

Table 1: Calculated amounts of carboxylic and amine groups on PEI-chitosan and raw materials.

Materials	Amounts of functional groups (mmol/g)		
	-COOH	$-NH_2$	-NH-
Chitosan	0	9.73	2.30
EDTA	10.1	0	0
PEI	0	21.1	15.0
PEI-chitosan(0:1)	5.38	0	2.44
PEI-chitosan(0.2:1)	1.91	2.01	2.33
PEI-chitosan(0.5:1)	1.43	4.53	3.96
PEI-chitosan(0.8:1)	1.95	4.24	4.15
PEI-chitosan(1:1)	1.74	4.44	4.14

Table 2: Comparison of the maximum adsorption capacities of La(III) onto various adsorbents.

Materials	q_m (mmol/g)	Ref.
Magnetic bentonite	0.132	[16]
Sodium beta-glycerophosphate modified cellulose	0.231	[70]
EDTA-β-cyclodextrin	0.343	[22]
Polydopamine coated PAN/PSF nanofiber	0.428	[67]
PEI-modified cellulose nanocrystals	0.611	[23]
Phosphoric acid modified activated carbon	1.262	[71]
PEI-chitosan(0.5:1)	2.015	this study
Mg–Fe-LDH-Cyanex-272	3.460	[20]

Table 3 The regeneration of PEI-chitosan (0.5:1) and 50-fold preconcentration of La(III) in the leachate of bauxite residue by using 1 M HNO_3 as eluent.

Run	La(III) conc. (mg/L)		RE%	La(III) conc. (mg/L)		Enrich factor
	Before adsorption	After adsorption		Eluent conc.	Eluate conc.	
1st	4.11	0.02	-	0	197.3	47.99
2nd	4.11	0.06	99.02	197.3	384.6	93.58
3rd	4.11	0.17	96.33	384.6	551.3	134.1
4th	4.11	0.40	90.71	551.3	706.7	171.9
5th	4.11	0.73	82.64	706.7	827.1	201.2
6th	4.11	1.24	70.17	827.1	918.4	223.5
10th	4.11	1.81	56.23	1152	1224	297.9

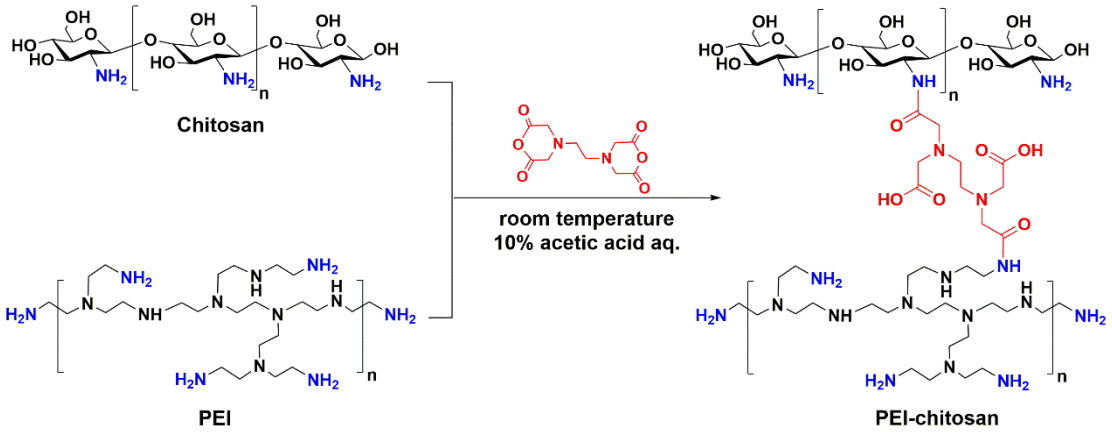

Fig. 1: Scheme for the synthesis of PEI-modified chitosan via EDTA dianhydride-mediated amidation reaction.

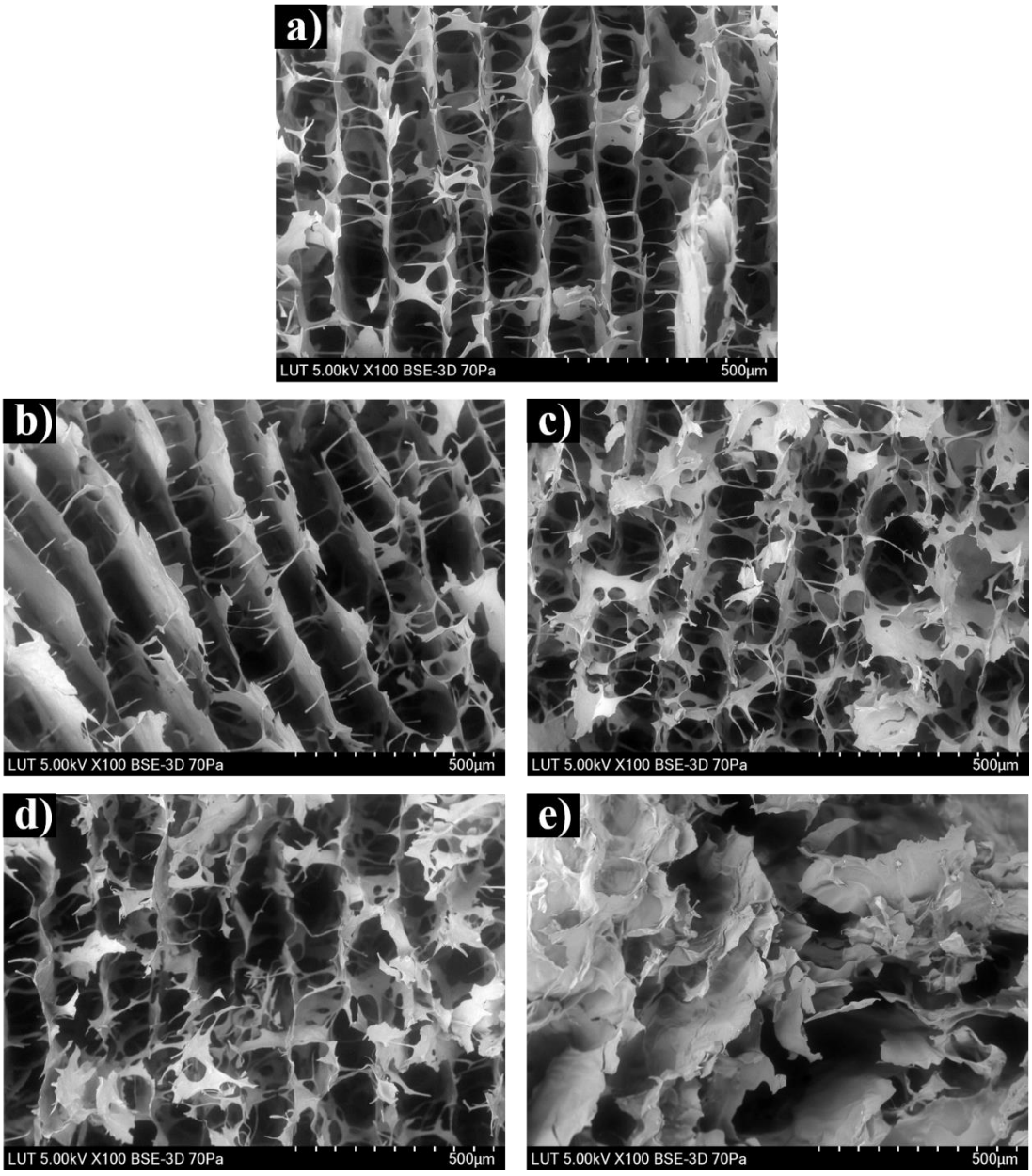

Fig. 2. SEM images of PEI-chitosan (0:1) (a), PEI-chitosan (0.2:1) (b), PEI-chitosan (0.5:1) (c), PEI-chitosan (0.8:1) (d), and PEI-chitosan (1:1) (e).

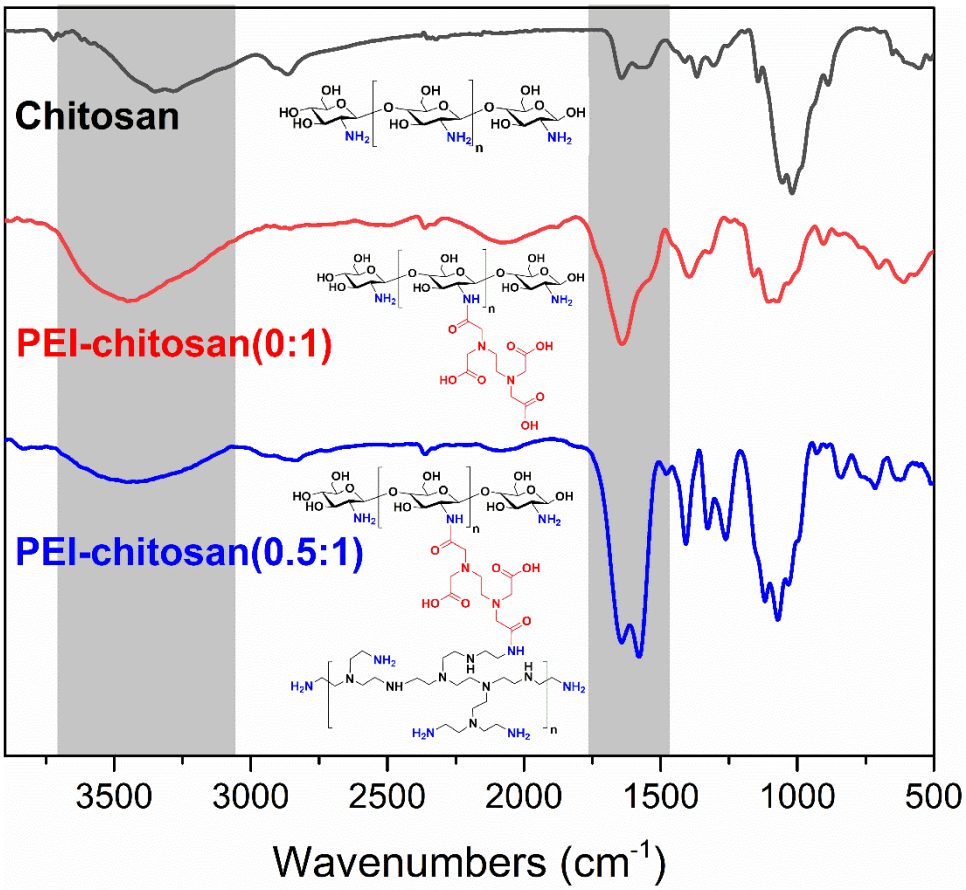

Fig. 3: FT-IR spectra of chitosan, PEI-chitosan(0:1), and PEI-chitosan(0.5:1).

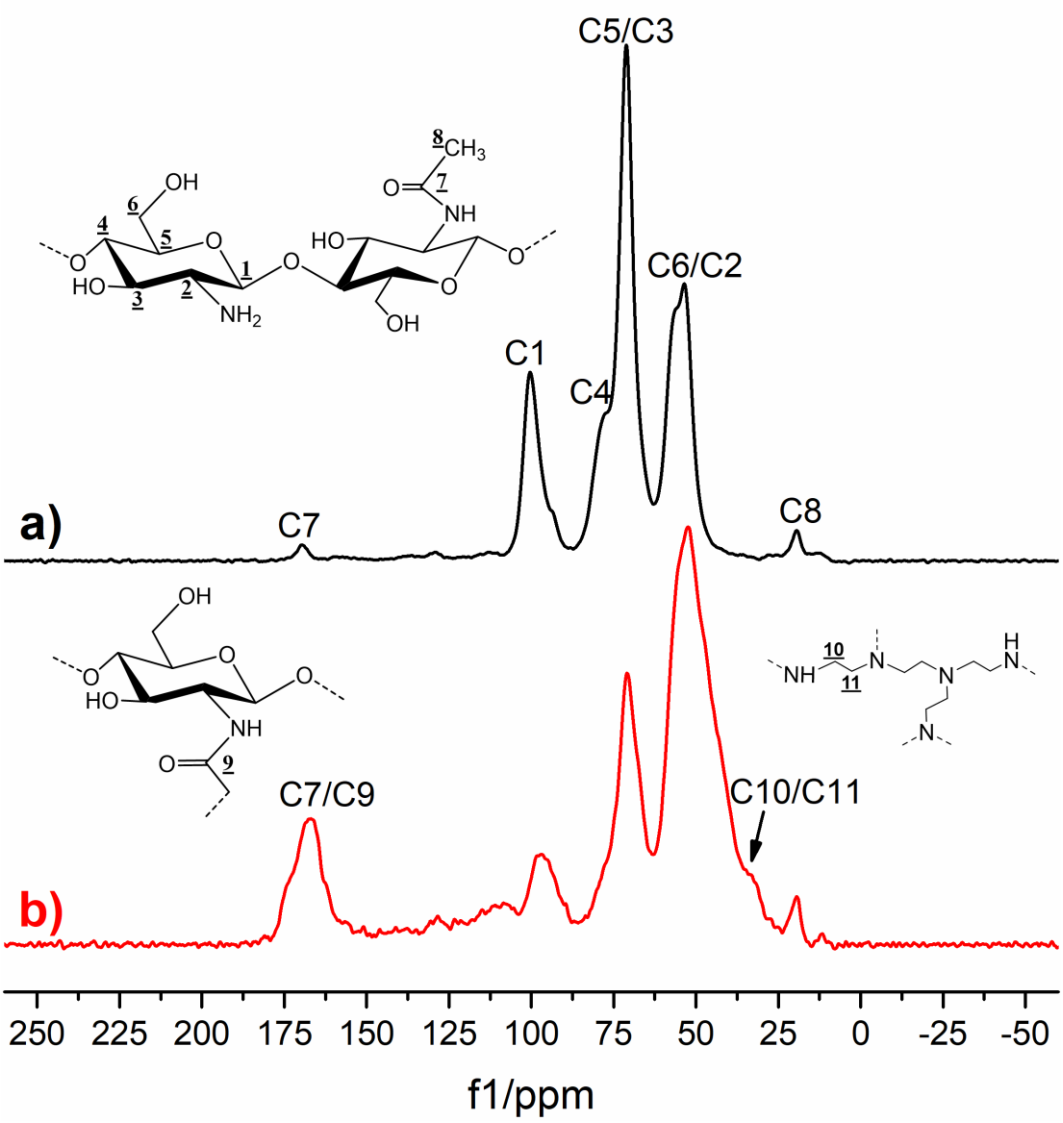

Fig. 4: The ^{13}C solid-state-MAS NMR spectra of chitosan (a) and PEI-chitosan (b).

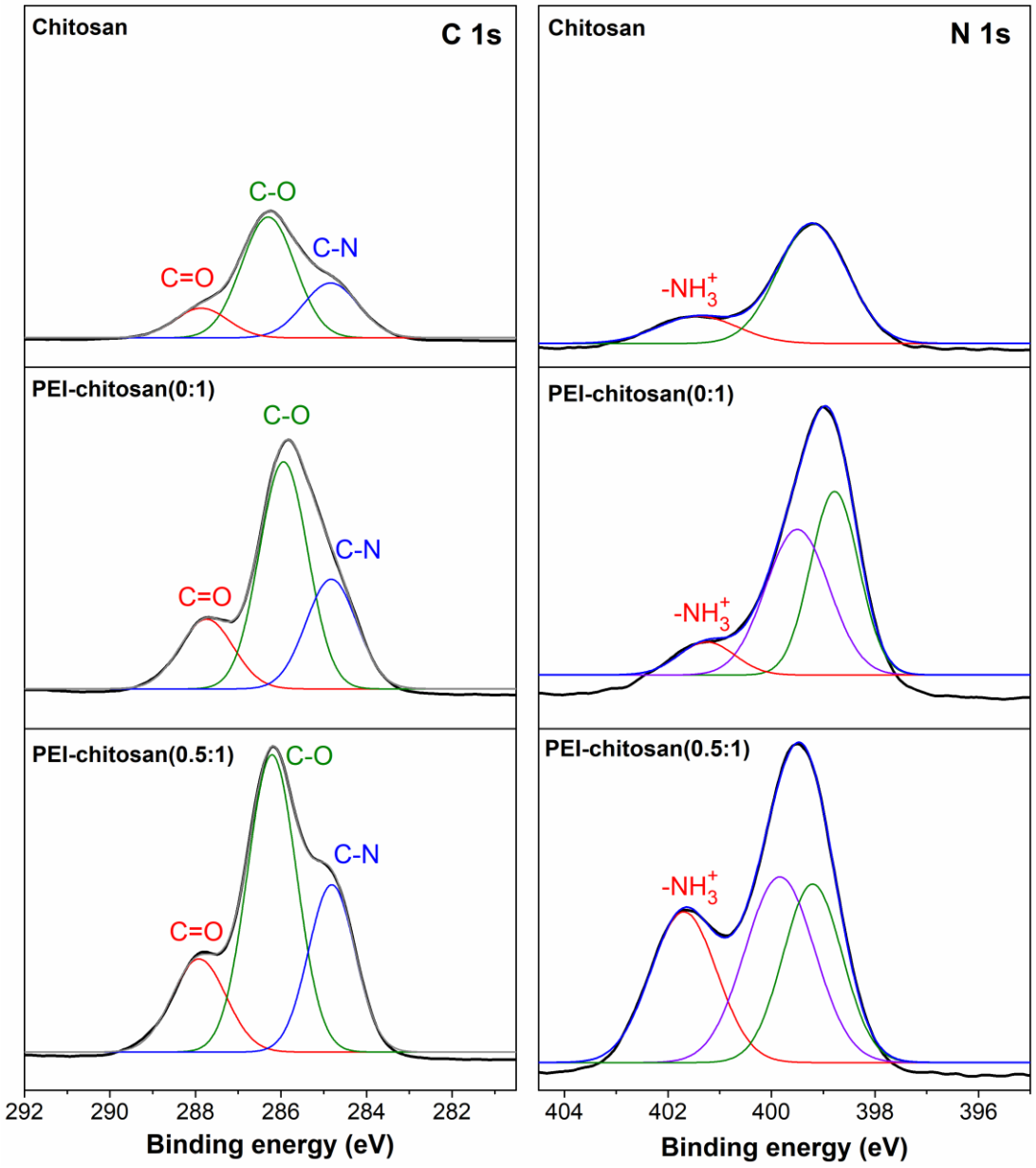

Fig. 5: Carbon and nitrogen core lines determined by XPS analysis for chitosan, PEI-chitosan (0:1), and PEI-chitosan (0.5:1).

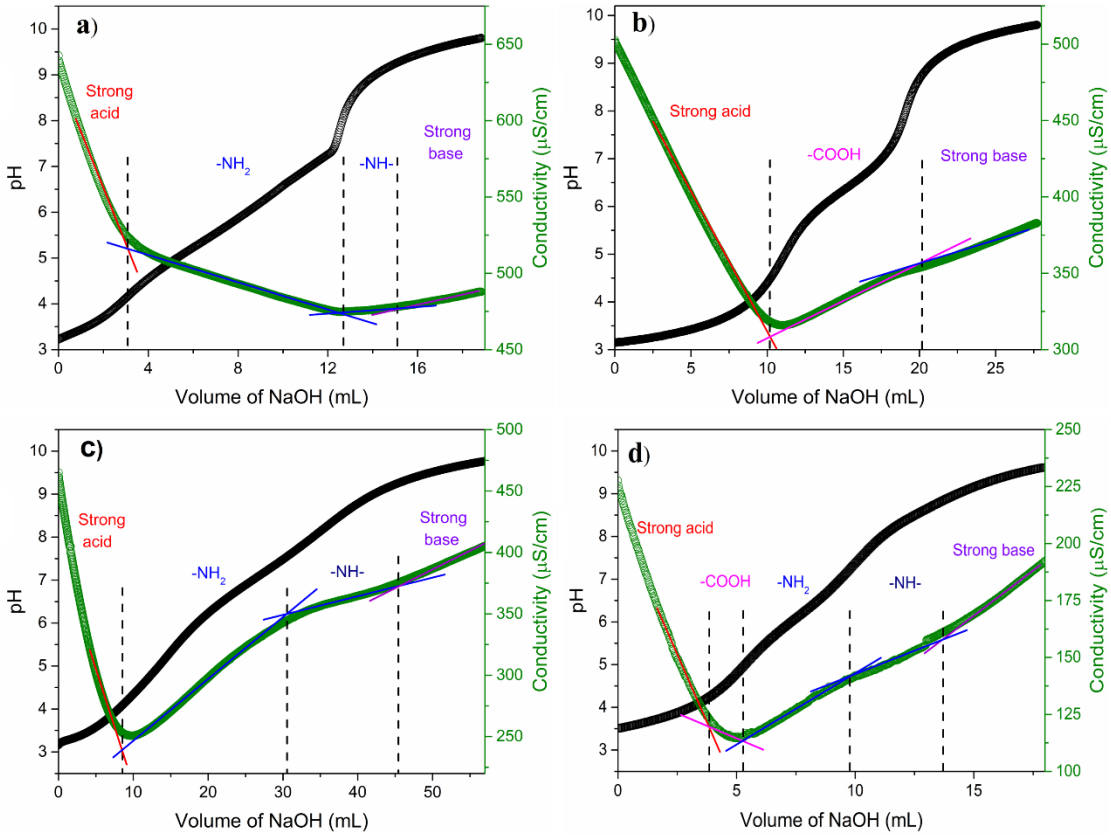

Fig. 6: Simultaneous conductometric-potentiometric titration curves of 0.025 wt% chitosan (a), EDTA (b), PEI (c), and PEI-chitosan (0.5:1) (d) by 0.01 M NaOH (PEI–chitosan material: 7-10 mg, volume: 40 mL, initial pH: 3, titration speed: 50 µL/min).

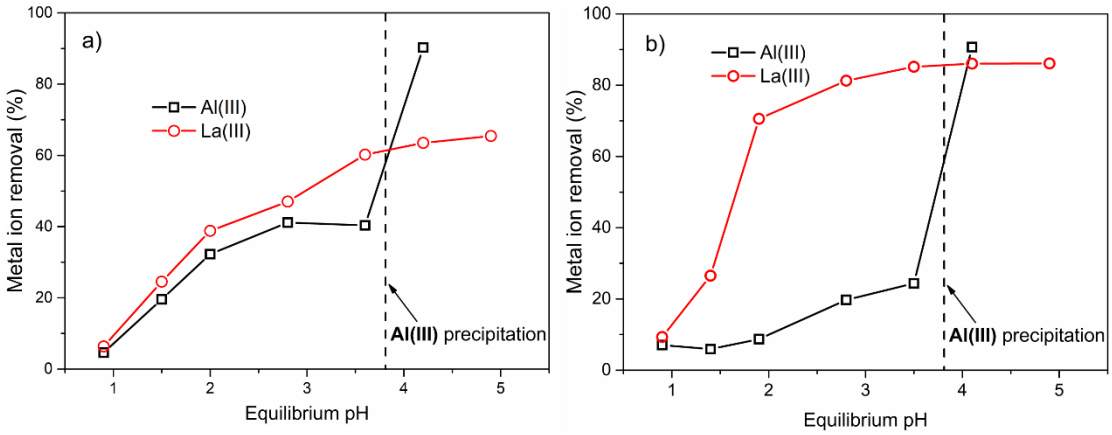

Fig. 7: Metal ion removal from a binary, equimolar solution of Al(III) and La(III) by PEI-chitosan (0:1) (a) and PEI-chitosan (0.5:1) (b). The vertical dashed line indicates the pH where the precipitation of Al(III) occurs (dosage: 1g/L, initial concentration of metal ions: 1 mM, contact time: 6 hr).

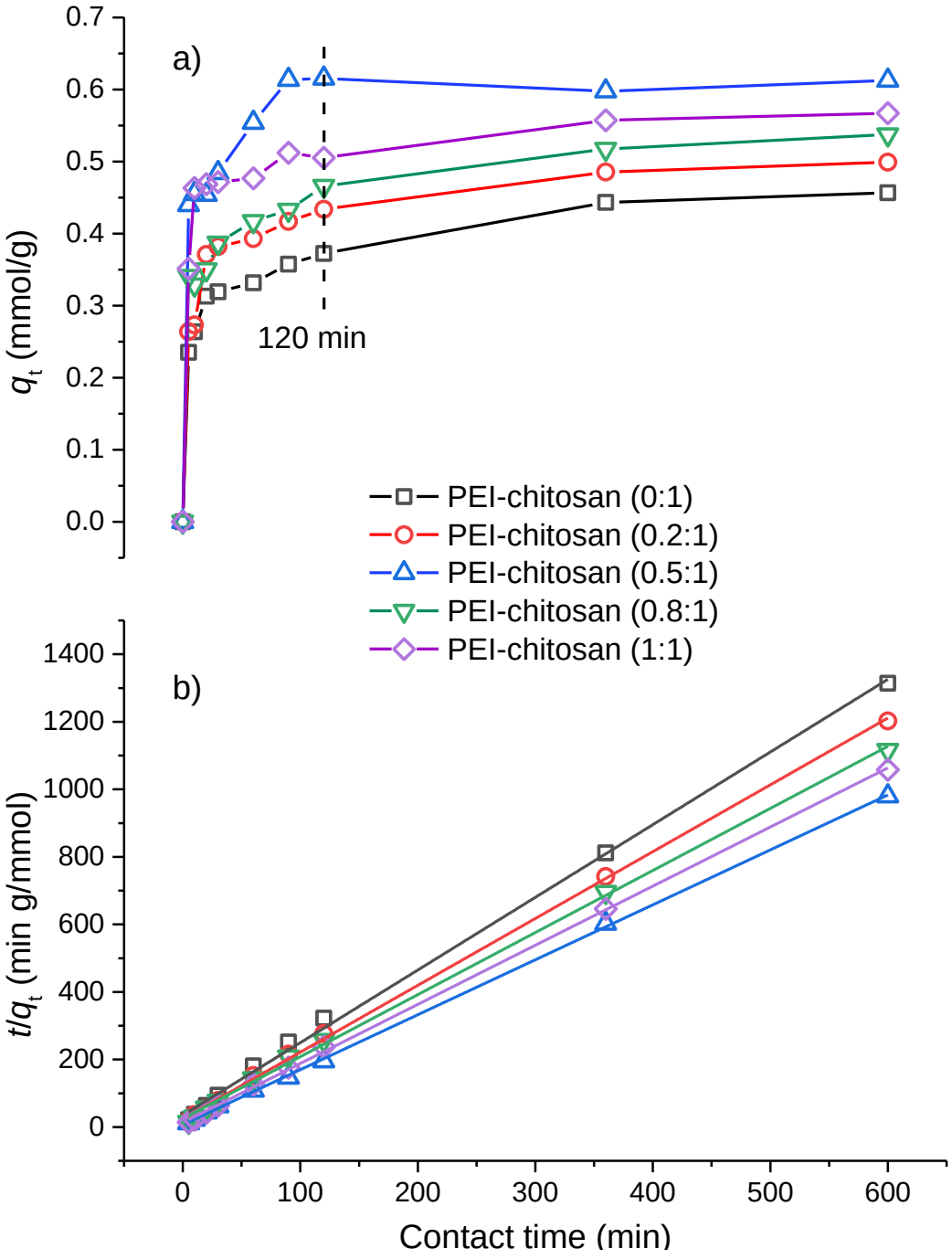

Fig. 8. Adsorption kinetics of La(III) onto PEI-chitosan (0:1), PEI-chitosan (0.2:1), PEI-chitosan (0.5:1), PEI-chitosan (0.8:1), and PEI-chitosan (1:1). Effect of contact time (a); Pseudo second-order fitting (lines, b) (dosage: 1g/L, initial concentration of La(III): 0.72 mM, pH: 3.5).

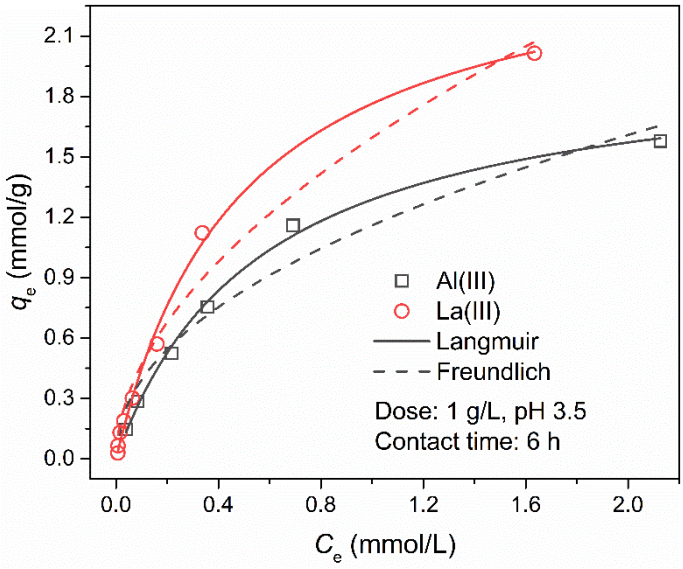

43

44

45 **Fig. 9:** Adsorption isotherms of single metal onto PEI-chitosan (0.5:1) according to

46 Langmuir and Freundlich models. Black solid/dashed lines for Al(III) fitting and red

47 lines for La(III) fitting.

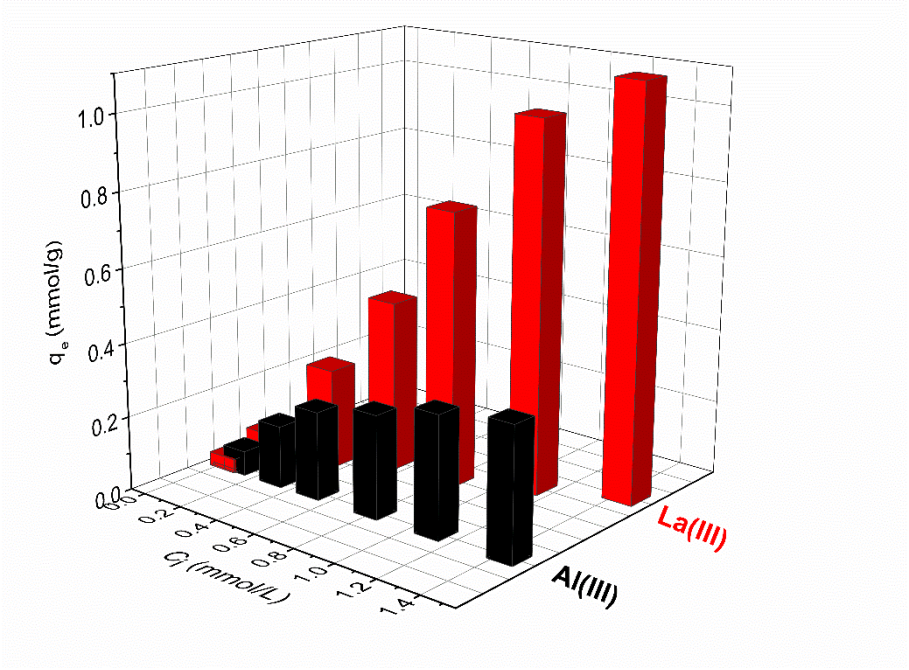

48

49

50 **Fig. 10:** Simultaneous adsorption of Al(III) and La(III) onto PEI-chitosan (0.5:1) in
51 equimolar Al(III)-La(III) binary system (25 °C, pH 3.5, adsorbent dose 1 g/L, and
52 contact time 6 h; The binary systems contain the equimolar initial La(III) and Al(III)
53 ranging from 0.04 to 1.4 mM).

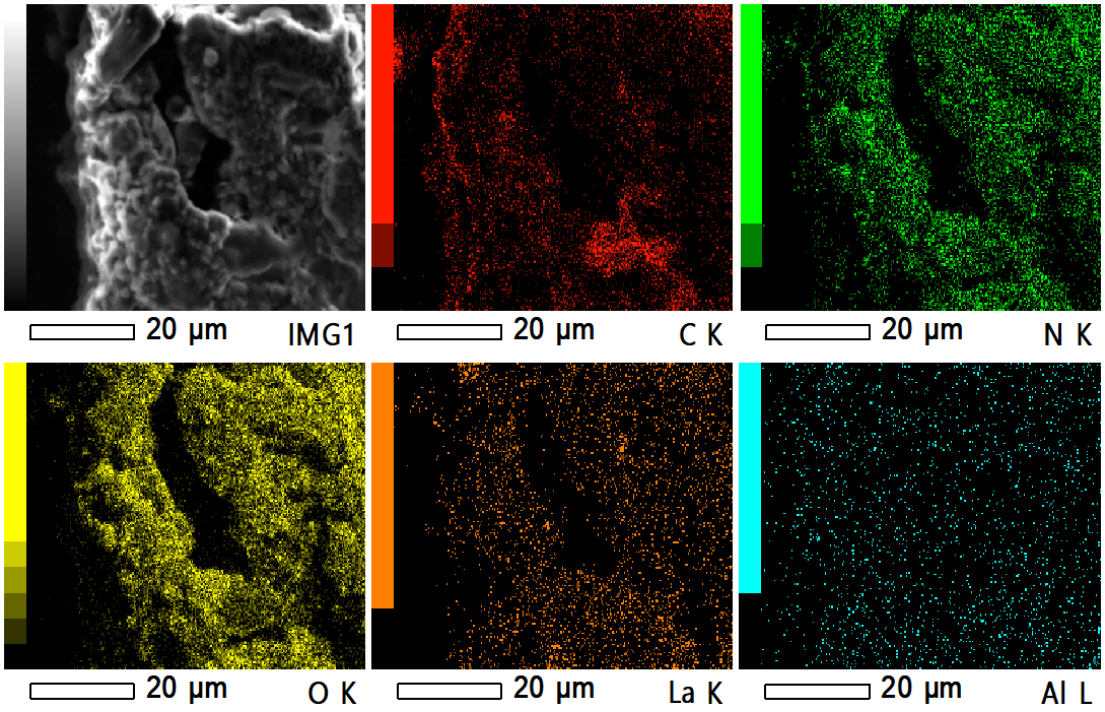

Fig. 11: SEM image and the EDS elemental distribution mapping of PEI-chitosan(0.5:1) after simultaneous adsorption of Al(III) and La(III). Initial concentration: 0.72 mmol/g Al(III) and La(III). Red spot: C signal; green spot: N signal; yellow spot: O signal; orange spot: La signal; light blue spot: Al signal.

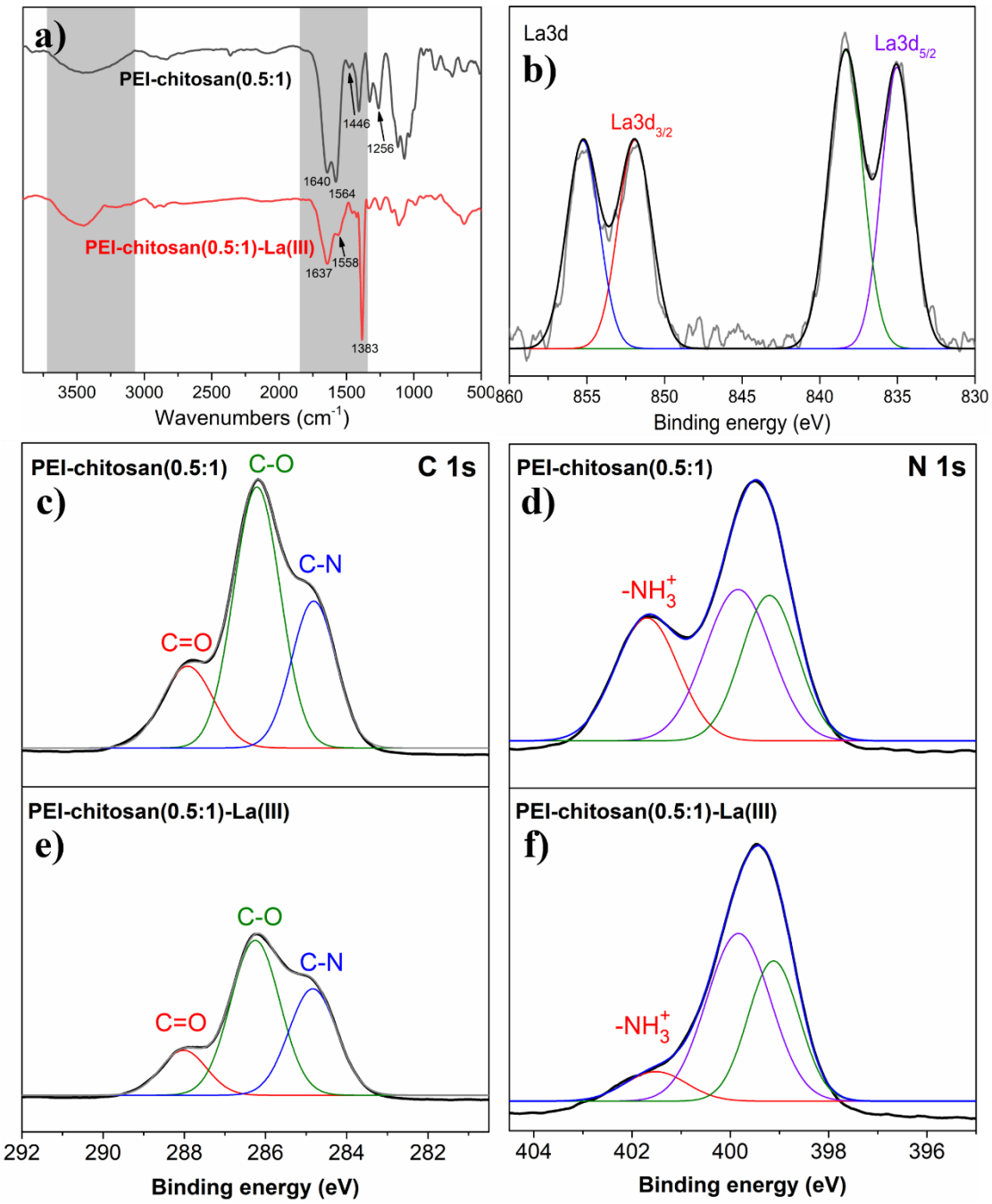

Fig. 12. FT-IR spectra of PEI-chitosan(0.5:1) before and after the adsorption of La(III) (a), La3d XPS spectrum of La(III) loaded on PEI-chitosan(0.5:1) (b), C1s XPS spectra of PEI-chitosan(0.5:1) before (c) and after (e) La(III) loading, N1s XPS spectra of PEI-chitosan(0.5:1) before (d) and after (f) La(III) loading.

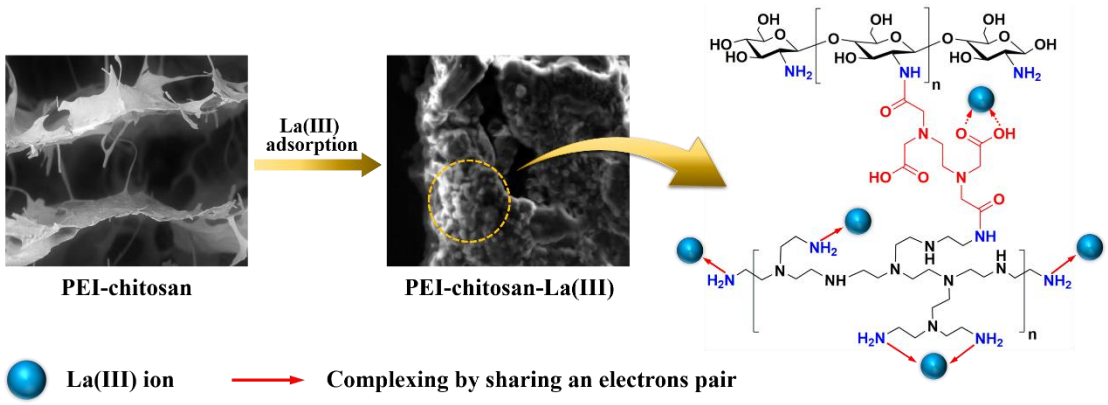

68

69

70 **Fig. 13:** Possible adsorption mechanisms for La(III) onto PEI-chitosan.

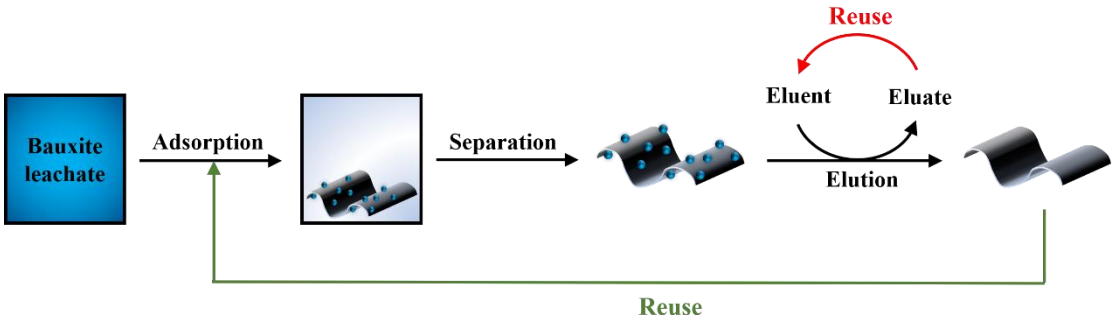

Fig. 14: Schematic diagram for the regeneration of spent PEI-chitosan(0.5:1) and preconcentration of La(III) via simultaneous recycling the adsorbent and eluent (dosage: 2 g/L, leachate volume: 500 mL, eluent volume: 10 mL).

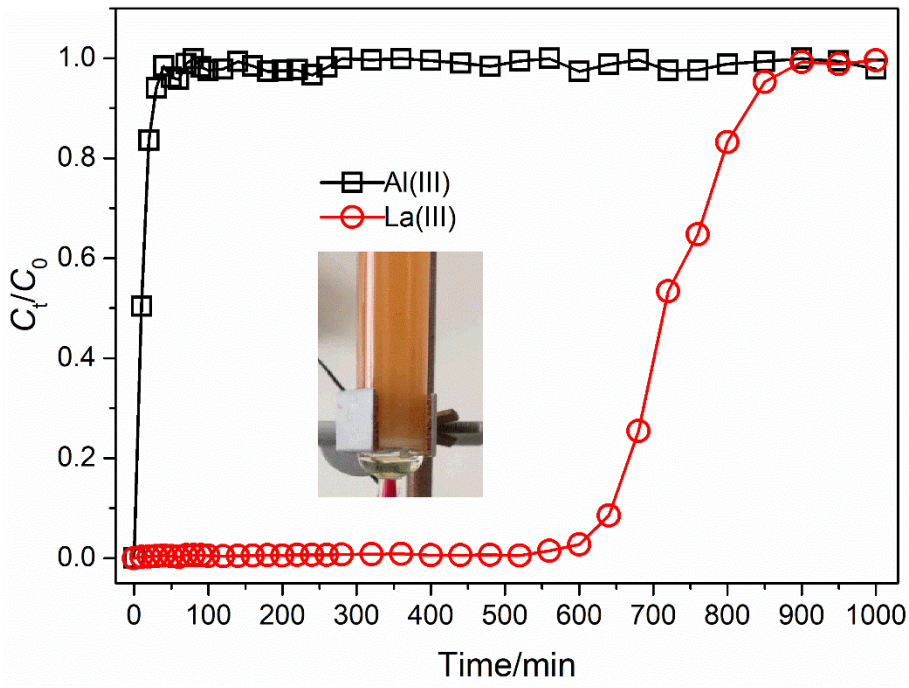

Fig. 15: Breakthrough curves of Al(III) and La(III) for a binary solution onto PEI-chitosan(0.5:1). Inset: the photo of the fixed-bed column. Column diameter 12 mm, bed height 70 mm, initial pH 3.5, and feed concentration of 330 mg/L for Al(III) and 4 mg/L for La(III) at a flow rate of 1 mL/min.

References

[1] Keith Veronese, Rare: The High-Stakes Race to Satisfy Our Need for the Scarcest Metals on Earth, New York, 2015.

[2] J. Roosen, K. Binnemans, Adsorption and chromatographic separation of rare earths with EDTA- and DTPA-functionalized chitosan biopolymers, J. Mater. Chem. A. 2 (2014) 1530–1540. doi:10.1039/C3TA14622G.

[3] J. Roosen, S. Van Roosendael, C.R. Borra, T. Van Gerven, S. Mullens, K. Binnemans, Recovery of scandium from leachates of Greek bauxite residue by adsorption on functionalized chitosan–silica hybrid materials, Green Chem. (2016) 2005–2013. doi:10.1039/C5GC02225H.

[4] H. Dong, J. Zhao, J. Chen, Y. Wu, B. Li, Recovery of platinum group metals from spent catalysts: A review, International Journal of Mineral Processing. 145 (2015) 108–113. doi:10.1016/j.minpro.2015.06.009.

[5] G. Power, M. Gräfe, C. Klauber, Bauxite residue issues: I. Current management, disposal and storage practices, Hydrometallurgy. 108 (2011) 33–45. doi:10.1016/j.hydromet.2011.02.006.

[6] Y. Xiong, Y. Gao, X. Guo, Y. Wang, X. Su, X. Sun, Water-Stable Metal-Organic Framework Material with Uncoordinated Terpyridine Site for Selective Th(IV)/Ln(III) Separation, ACS Sustainable Chemistry and Engineering. 7 (2019) 3120–3126. doi:10.1021/acssuschemeng.8b04875.

[7] Horizon 2020, European Training Network for Zero-Waste Valorisation of Bauxite Residue (Red Mud), WordPress. (2019).

https://etn.redmud.org/project/.

[8] K. Evans, The History, Challenges, and New Developments in the Management and Use of Bauxite Residue, Journal of Sustainable Metallurgy. 2 (2016) 316–331. doi:10.1007/s40831-016-0060-x.

[9] K. Binnemans, P.T. Jones, B. Blanpain, T. Van Gerven, Y. Pontikes, Towards zero-waste valorisation of rare-earth-containing industrial process residues: A critical review, Journal of Cleaner Production. 99 (2015) 17–38. doi:10.1016/j.jclepro.2015.02.089.

[10] C.R. Borra, B. Blanpain, Y. Pontikes, K. Binnemans, T. Van Gerven, Recovery of Rare Earths and Major Metals from Bauxite Residue (Red Mud) by Alkali Roasting, Smelting, and Leaching, Journal of Sustainable Metallurgy. 3 (2017) 393–404. doi:10.1007/s40831-016-0103-3.

[11] C. Klauber, M. Gräfe, G. Power, Bauxite residue issues: II. options for residue utilization, Hydrometallurgy. 108 (2011) 11–32. doi:10.1016/j.hydromet.2011.02.007.

[12] S.-M. Alatalo, F.D. Pileidis, E. Mäkilä, M. Sevilla, E. Repo, J.J. Salonen, M. Sillanpää, M.-M. Titirici, Versatile cellulose based carbon aerogel for the removal of both cationic and anionic metal contaminants from water, ACS Applied Materials & Interfaces. (2015) acsami.5b08287. doi:10.1021/acsami.5b08287.

[13] A. Duran, M. Tuzen, M. Soylak, Preconcentration of some trace elements via using multiwalled carbon nanotubes as solid phase extraction adsorbent,

Journal of Hazardous Materials. 169 (2009) 466–471. doi:10.1016/j.jhazmat.2009.03.119.

[14] B.K. Esser, A. Volpe, J.M. Kenneally, D.K. Smith, Preconcentration and Purification of Rare Earth Elements in Natural Waters Using Silica-Immobilized 8-Hydroxyquinoline and a Supported Organophosphorus Extractant, Analytical Chemistry. 66 (1994) 1736–1742. doi:10.1021/ac00082a022.

[15] J.-Y. Yang, B.-Y. Yue, J.-T. Jie-Teng, Q. Liu, X.-Y. Jiang, M. Zhong, F.-L. Zhou, J.-G. Yu, Dichlrocarbene modified graphene oxide nanocomposite fabricated by a facile hydrothermal method and its adsorption properties towards rare earth elements, Desalination and Water Treatmentater Treatment. 162 (2019) 260–268. doi:10.5004/dwt.2019.24300.

[16] D. Wu, C. Zhu, Y. Chen, B. Zhu, Y. Yang, Q. Wang, W. Ye, Preparation, characterization and adsorptive study of rare earth ions using magnetic GMZ bentonite, Applied Clay Science. 62–63 (2012) 87–93. doi:10.1016/j.clay.2012.04.015.

[17] G.A. Moldoveanu, V.G. Papangelakis, Recovery of rare earth elements adsorbed on clay minerals: I. Desorption mechanism, Hydrometallurgy. 117–118 (2012) 71–78. doi:10.1016/j.hydromet.2012.02.007.

[18] F. Granados-Correa, J. Vilchis-Granados, M. Jiménez-Reyes, L.A. Quiroz-Granados, Adsorption Behaviour of La(III) and Eu(III) Ions from Aqueous Solutions by Hydroxyapatite: Kinetic, Isotherm, and Thermodynamic

Studies, Journal of Chemistry. 2013 (2013) 1–9. doi:10.1155/2013/751696.

[19] Y.-J. Tu, C.T. Johnston, Rapid recovery of rare earth elements in industrial wastewater by $CuFe_2O_4$ synthesized from Cu sludge, Journal of Rare Earths. 36 (2018) 513–520. doi:10.1016/j.jre.2017.11.009.

[20] M.S. Gasser, M.I. Aly, Separation and recovery of rare earth elements from spent nickel-metal-hydride batteries using synthetic adsorbent, International Journal of Mineral Processing. 121 (2013) 31–38. doi:10.1016/j.minpro.2013.02.012.

[21] H. Veisi, S. Taheri, S. Hemmati, Preparation of polydopamine sulfamic acid-functionalized magnetic Fe_3O_4 nanoparticles with a core/shell nanostructure as heterogeneous and recyclable nanocatalysts for the acetylation of alcohols, phenols, amines and thiols under solvent-free conditions, Green Chemistry. 18 (2016) 6337–6348. doi:10.1039/C6GC01975G.

[22] F. Zhao, E. Repo, Y. Meng, X. Wang, D. Yin, M. Sillanpää, An EDTA-β-cyclodextrin material for the adsorption of rare earth elements and its application in preconcentration of rare earth elements in seawater, Journal of Colloid and Interface Science. 465 (2016) 215–224. doi:10.1016/j.jcis.2015.11.069.

[23] F. Zhao, E. Repo, Y. Song, D. Yin, S. Ben Hammouda, L. Chen, S. Kalliola, J. Tang, K.C. Tam, M. Sillanpää, Polyethylenimine-cross-linked cellulose nanocrystals for highly efficient recovery of rare earth elements from water and a mechanism study, Green Chemistry. 19 (2017) 4816–4828.

184 doi:10.1039/C7GC01770G.
185 [24] E. Repo, J.K. Warchol, T.A. Kurniawan, M.E.T. Sillanpää, Adsorption of Co(II)
186 and Ni(II) by EDTA- and/or DTPA-modified chitosan: Kinetic and equilibrium
187 modeling, Chemical Engineering Journal. 161 (2010) 73–82.
188 doi:10.1016/j.cej.2010.04.030.
189 [25] F. Zhao, E. Repo, M. Sillanpää, Y. Meng, D. Yin, W.Z. Tang, Green Synthesis
190 of Magnetic EDTA- and/or DTPA-Cross-Linked Chitosan Adsorbents for
191 Highly Efficient Removal of Metals, Industrial & Engineering Chemistry
192 Research. 54 (2015) 1271–1281. doi:10.1021/ie503874x.
193 [26] F. Zhao, E. Repo, D. Yin, M.E.T. Sillanpää, Adsorption of Cd(II) and Pb(II) by
194 a novel EGTA-modified chitosan material: Kinetics and isotherms, Journal of
195 Colloid and Interface Science. 409 (2013) 174–182.
196 [27] L. Gao, D. Minakata, Z. Wei, R. Spinney, D.D. Dionysiou, C.-J. Tang, L. Chai,
197 R. Xiao, Mechanistic Study on the Role of Soluble Microbial Products in
198 Sulfate Radical-Mediated Degradation of Pharmaceuticals, Environmental
199 Science & Technology. 53 (2019) 342–353. doi:10.1021/acs.est.8b05129.
200 [28] L. Melone, B. Rossi, N. Pastori, W. Panzeri, A. Mele, C. Punta,
201 TEMPO-Oxidized Cellulose Cross-Linked with Branched Polyethyleneimine:
202 Nanostructured Adsorbent Sponges for Water Remediation, ChemPlusChem.
203 80 (2015) 1408–1415. doi:10.1002/cplu.201500145.
204 [29] O. Boussif, F. Lezoualc'h, M.A. Zanta, M.D. Mergny, D. Scherman, B.
205 Demeneix, J.P. Behr, A versatile vector for gene and oligonucleotide transfer

into cells in culture and in vivo: polyethylenimine., Proceedings of the National Academy of Sciences. 92 (1995) 7297–7301. doi:10.1073/pnas.92.16.7297.

[30] Y. Chen, B. Pan, H. Li, W. Zhang, L. Lv, J. Wu, Selective Removal of Cu(II) Ions by Using Cation-exchange Resin-Supported Polyethyleneimine (PEI) Nanoclusters, Environmental Science & Technology. 44 (2010) 3508–3513. doi:10.1021/es100341x.

[31] M. Gericke, J. Trygg, P. Fardim, Functional Cellulose Beads: Preparation, Characterization, and Applications, Chemical Reviews. 113 (2013) 4812–4836. doi:10.1021/cr300242j.

[32] Z. Huang, Z. Li, L. Zheng, L. Zhou, Z. Chai, X. Wang, W. Shi, Interaction mechanism of uranium(VI) with three-dimensional graphene oxide-chitosan composite: Insights from batch experiments, IR, XPS, and EXAFS spectroscopy, Chemical Engineering Journal. 328 (2017) 1066–1074. doi:10.1016/j.cej.2017.07.067.

[33] M. Wang, T. Liu, L. Han, W. Gao, S. Yang, N. Zhang, Functionalized O-carboxymethyl-chitosan/polyethylenimine based novel dual pH-responsive nanocarriers for controlled co-delivery of DOX and genes, Polymer Chemistry. 6 (2015) 3324–3335. doi:10.1039/C5PY00013K.

[34] Y.Y. Yu, Z. Wang, L. Cai, G. Wang, X. Yang, X.P. Wan, X.H. Xu, Y. Li, R. Gao, Synthesis and characterization of methoxy poly(ethylene glycol)-O-chitosan-polyethylenimine for gene delivery, Carbohydrate Polymers. 81 (2010) 269–274. doi:10.1016/j.carbpol.2010.02.018.

[35] M.S. Huh, S.-Y. Lee, S. Park, S. Lee, H. Chung, S. Lee, Y. Choi, Y.-K. Oh, J.H. Park, S.Y. Jeong, K. Choi, K. Kim, I.C. Kwon, Tumor-homing glycol chitosan/polyethylenimine nanoparticles for the systemic delivery of siRNA in tumor-bearing mice, Journal of Controlled Release. 144 (2010) 134–143. doi:10.1016/j.jconrel.2010.02.023.

[36] L. You, C. Huang, F. Lu, A. Wang, X. Liu, Q. Zhang, Facile synthesis of high performance porous magnetic chitosan - polyethylenimine polymer composite for Congo red removal, International Journal of Biological Macromolecules. 107 (2018) 1620–1628. doi:10.1016/j.ijbiomac.2017.10.025.

[37] F. Zhao, E. Repo, D. Yin, Y. Meng, S. Jafari, M. Sillanpää, EDTA-Cross-Linked β-Cyclodextrin: An Environmentally Friendly Bifunctional Adsorbent for Simultaneous Adsorption of Metals and Cationic Dyes, Environmental Science & Technology. 49 (2015) 10570–10580. doi:10.1021/acs.est.5b02227.

[38] H. Zeng, L. Wang, D. Zhang, P. Yan, J. Nie, V.K. Sharma, C. Wang, Highly efficient and selective removal of mercury ions using hyperbranched polyethylenimine functionalized carboxymethyl chitosan composite adsorbent, Chemical Engineering Journal. 358 (2019) 253–263. doi:10.1016/j.cej.2018.10.001.

[39] M. Musielak, A. Gagor, B. Zawisza, E. Talik, R. Sitko, Graphene Oxide/Carbon Nanotube Membranes for Highly Efficient Removal of Metal Ions from Water, ACS Applied Materials & Interfaces. (2019).

250 doi:10.1021/acsami.9b11214.
251 [40] J. Tang, Y. Song, F. Zhao, S. Spinney, J. da Silva Bernardes, K.C. Tam,
252 Compressible cellulose nanofibril (CNF) based aerogels produced via a
253 bio-inspired strategy for heavy metal ion and dye removal, Carbohydrate
254 Polymers. 208 (2019) 404–412. doi:10.1016/j.carbpol.2018.12.079.
255 [41] J. Zhao, C. Lu, X. He, X. Zhang, W. Zhang, X. Zhang,
256 Polyethylenimine-Grafted Cellulose Nanofibril Aerogels as Versatile Vehicles
257 for Drug Delivery, ACS Applied Materials & Interfaces. 7 (2015) 2607–2615.
258 doi:10.1021/am507601m.
259 [42] C. Ling, X. Li, Z. Zhang, F. Liu, Y. Deng, X. Zhang, A. Li, L. He, B. Xing,
260 High Adsorption of Sulfamethoxazole by an Amine-Modified Polystyrene–
261 Divinylbenzene Resin and Its Mechanistic Insight, Environmental Science &
262 Technology. 50 (2016) 10015–10023. doi:10.1021/acs.est.6b02846.
263 [43] L.V.A. Gurgel, L.F. Gil, Adsorption of Cu(II), Cd(II) and Pb(II) from aqueous
264 single metal solutions by succinylated twice-mercerized sugarcane bagasse
265 functionalized with triethylenetetramine, Water Research. 43 (2009) 4479–
266 4488. doi:10.1016/j.watres.2009.07.017.
267 [44] I. Kavianinia, P.G. Plieger, N.G. Kandile, D.R.K. Harding, Fixed-bed column
268 studies on a modified chitosan hydrogel for detoxification of aqueous solutions
269 from copper (II), Carbohydrate Polymers. 90 (2012) 875–886.
270 doi:10.1016/j.carbpol.2012.06.014.
271 [45] G. Lawrie, I. Keen, B. Drew, A. Chandler-Temple, L. Rintoul, P. Fredericks, L.

272 Grøndahl, Interactions between Alginate and Chitosan Biopolymers
273 Characterized Using FTIR and XPS, Biomacromolecules. 8 (2007) 2533–2541.
274 doi:10.1021/bm070014y.
275 [46] L. Vanzetti, L. Pasquardini, C. Potrich, V. Vaghi, E. Battista, F. Causa, C.
276 Pederzolli, XPS analysis of genomic DNA adsorbed on PEI-modified surfaces,
277 Surface and Interface Analysis. 48 (2016) 611–615. doi:10.1002/sia.5932.
278 [47] Y. Ding, B.-Q. Miao, Y.-C. Jiang, H.-C. Yao, X.-F. Li, Y. Chen,
279 Polyethylenimine-modified nickel phosphide nanosheets: interfacial protons
280 boost the hydrogen evolution reaction, Journal of Materials Chemistry A. 7
281 (2019) 13770–13776. doi:10.1039/C9TA04283K.
282 [48] T.B. Mostafa, Chemical modification of polypropylene fibers grafted vinyl
283 imidazole/acrylonitrile copolymer prepared by gamma radiation and its
284 possible use for the removal of some heavy metal ions, Journal of Applied
285 Polymer Science. 111 (2009) 11–18. doi:10.1002/app.26850.
286 [49] Y. Hu, L.C. Misal Castro, E. Drouin, J. Florek, H. Kählig, D. Larivière, F.
287 Kleitz, F.-G. Fontaine, Size-Selective Separation of Rare Earth Elements Using
288 Functionalized Mesoporous Silica Materials, ACS Applied Materials &
289 Interfaces. 11 (2019) 23681–23691. doi:10.1021/acsami.9b04183.
290 [50] J. Sánchez-España, I. Yusta, M. Diez-Ercilla, Schwertmannite and
291 hydrobasaluminite: A re-evaluation of their solubility and control on the iron
292 and aluminium concentration in acidic pit lakes, Applied Geochemistry. 26
293 (2011) 1752–1774. doi:10.1016/j.apgeochem.2011.06.020.

[51] K. Stone, A.M.T.S. Bandara, G. Senanayake, S. Jayasekera, Processing of rare earth phosphate concentrates: A comparative study of pre-leaching with perchloric, hydrochloric, nitric and phosphoric acids and deportment of minor/major elements, Hydrometallurgy. 163 (2016) 137–147. doi:10.1016/j.hydromet.2016.03.014.

[52] Chelate Table of Stability Constants, (n.d.). https://www.dojindo.com/Images/Product Photo/Chelate_Table_of_Stability_Constants.pdf.

[53] J.C. Callura, K.M. Perkins, J.P. Baltrus, N.R. Washburn, D.A. Dzombak, A.K. Karamalidis, Adsorption kinetics, thermodynamics, and isotherm studies for functionalized lanthanide-chelating resins, Journal of Colloid and Interface Science. 557 (2019) 465–477. doi:10.1016/j.jcis.2019.08.097.

[54] R. V. Rodrigues, Ł. Marciniak, L.U. Khan, A.A.L. Marins, R. Tomala, E.J.B. Muri, J.R. Matos, W. Stręk, Synthesis, photoluminescence properties and thermal investigation by TG-MS of $RE(DAS)_3 \cdot xH_2O$ (RE = Eu^{3+}, Tb^{3+}), Journal of Rare Earths. 37 (2019) 1164–1169. doi:10.1016/j.jre.2019.01.006.

[55] A.E. Martell, R.M. Smith, Critical Stability Constants, Plenum Press, New York, 1974.

[56] R. Xiao, K. Liu, L. Bai, D. Minakata, Y. Seo, R. Kaya Göktaş, D.D. Dionysiou, C.-J. Tang, Z. Wei, R. Spinney, Inactivation of pathogenic microorganisms by sulfate radical: Present and future, Chemical Engineering Journal. 371 (2019) 222–232. doi:10.1016/j.cej.2019.03.296.

316 [57] R. Xiao, L. He, Z. Luo, R. Spinney, Z. Wei, D.D. Dionysiou, F. Zhao, An
317 experimental and theoretical study on the degradation of clonidine by hydroxyl
318 and sulfate radicals, Science of The Total Environment. 710 (2020) 136333.
319 doi:10.1016/j.scitotenv.2019.136333.
320 [58] M. Li, F. Zhao, M. Sillanpää, Y. Meng, D. Yin, Electrochemical degradation of
321 2-diethylamino-6-methyl-4-hydroxypyrimidine using three-dimensional
322 electrodes reactor with ceramic particle electrodes, Separation and Purification
323 Technology. 156 (2015) 588–595. doi:10.1016/j.seppur.2015.10.053.
324 [59] Y.. Ho, G. McKay, Pseudo-second order model for sorption processes, Process
325 Biochemistry. 34 (1999) 451–465. doi:10.1016/S0032-9592(98)00112-5.
326 [60] X. Min, W. Li, Z. Wei, R. Spinney, D.D. Dionysiou, Y. Seo, C.-J. Tang, Q. Li,
327 R. Xiao, Sorption and biodegradation of pharmaceuticals in aerobic activated
328 sludge system: A combined experimental and theoretical mechanistic study,
329 Chemical Engineering Journal. 342 (2018) 211–219.
330 doi:10.1016/j.cej.2018.01.012.
331 [61] Z. Wei, W. Li, D. Zhao, Y. Seo, R. Spinney, D.D. Dionysiou, Y. Wang, W. Zeng,
332 R. Xiao, Electrophilicity index as a critical indicator for the biodegradation of
333 the pharmaceuticals in aerobic activated sludge processes, Water Research. 160
334 (2019) 10–17. doi:10.1016/j.watres.2019.05.057.
335 [62] R. Xiao, J. Ma, Z. Luo, W. Zeng, Z. Wei, R. Spinney, W. Hu, D.D. Dionysiou,
336 Experimental and theoretical insight into hydroxyl and sulfate
337 radicals-mediated degradation of carbamazepine, Environmental Pollution.

(2019) 113498. doi:10.1016/j.envpol.2019.113498.

[63] Z. Huang, Z. Li, L. Zheng, L. Zhou, Z. Chai, X. Wang, W. Shi, Interaction mechanism of uranium(VI) with three-dimensional graphene oxide-chitosan composite: Insights from batch experiments, IR, XPS, and EXAFS spectroscopy, Chemical Engineering Journal. 328 (2017) 1066–1074. doi:10.1016/j.cej.2017.07.067.

[64] G. Hong, M. Wang, X. Li, L. Shen, X. Wang, M. Zhu, B.S. Hsiao, Micro-nano structure nanofibrous p-sulfonatocalix[8]arene complex membranes for highly efficient and selective adsorption of lanthanum(iii) ions in aqueous solution, RSC Advances. 5 (2015) 21178–21188. doi:10.1039/c5ra02423d.

[65] Y. Yan, Q. An, Z. Xiao, W. Zheng, S. Zhai, Flexible core-shell/bead-like alginate@PEI with exceptional adsorption capacity, recycling performance toward batch and column sorption of Cr(VI), Chemical Engineering Journal. 313 (2017) 475–486. doi:10.1016/j.cej.2016.12.099.

[66] R.S. Vieira, M.L.M. Oliveira, E. Guibal, E. Rodríguez-Castellón, M.M. Beppu, Copper, mercury and chromium adsorption on natural and crosslinked chitosan films: An XPS investigation of mechanism, Colloids and Surfaces A: Physicochemical and Engineering Aspects. 374 (2011) 108–114. doi:10.1016/j.colsurfa.2010.11.022.

[67] G. Hong, L. Shen, M. Wang, Y. Yang, X. Wang, M. Zhu, B.S. Hsiao, Nanofibrous polydopamine complex membranes for adsorption of Lanthanum (III) ions, Chemical Engineering Journal. 244 (2014) 307–316.

360 doi:10.1016/j.cej.2014.01.073.
361 [68] Y. Ren, H.A. Abbood, F. He, H. Peng, K. Huang, Magnetic EDTA-modified
362 chitosan/SiO2/Fe3O4 adsorbent: Preparation, characterization, and application
363 in heavy metal adsorption, Chemical Engineering Journal. 226 (2013) 300–311.
364 doi:10.1016/j.cej.2013.04.059.
365 [69] I. Kursun, T.D. Tombal, M. Terzi, Solubility of Eskisehir thorium/rare earth
366 ores in sulphuric and nitric acids, Physicochemical Problems of Mineral
367 Processing. 54 (2018) 476–483. doi:10.5277/ppmp1846.
368 [70] A. Gabor, C.M. Davidescu, A. Negrea, M. Ciopec, I. Grozav, P. Negrea, N.
369 Duteanu, Optimizing the lanthanum adsorption process onto chemically modi fi
370 ed biomaterials using factorial and response surface design, Journal of
371 Environmental Management. 204 (2017) 839–844.
372 doi:10.1016/j.jenvman.2017.01.046.
373 [71] N.S. Awwad, H.M.H. Gad, M.I. Ahmad, H.F. Aly, Sorption of lanthanum and
374 erbium from aqueous solution by activated carbon prepared from rice husk,
375 Colloids and Surfaces B: Biointerfaces. 81 (2010) 593–599.
376 doi:10.1016/j.colsurfb.2010.08.002.
377